

ornl

ORNL/TM-10709

**OAK RIDGE
NATIONAL
LABORATORY**

MARTIN MARIETTA

**Micromechanisms of Deformation
and Fracture in Ordered
Intermetallic Alloys -
I. Strengthening Mechanisms**

M. H. Yoo
J. A. Horton
C.T. Liu

OAK RIDGE NATIONAL LABORATORY
CENTRAL RESEARCH LIBRARY
CIRCULATION SERVICES
OAK RIDGE, TENN. 37831
LIBRARY LOAN COPY
DO NOT TRANSFER TO ANOTHER PERSON
If you wish someone else to see this
report, send in note with report and
the library will arrange a loan.

OPERATED BY
MARTIN MARIETTA ENERGY SYSTEMS, INC.
FOR THE UNITED STATES
DEPARTMENT OF ENERGY

Printed in the United States of America. Available from
National Technical Information Service
U.S. Department of Commerce
5285 Port Royal Road, Springfield, Virginia 22161
NTIS price codes—Printed Copy: A04 Microfiche A01

This report was prepared as an account of work sponsored by an agency of the United States Government. Neither the United States Government nor any agency thereof, nor any of their employees, makes any warranty, express or implied, or assumes any legal liability or responsibility for the accuracy, completeness, or usefulness of any information, apparatus, product, or process disclosed, or represents that its use would not infringe privately owned rights. Reference herein to any specific commercial product, process, or service by trade name, trademark, manufacturer, or otherwise, does not necessarily constitute or imply its endorsement, recommendation, or favoring by the United States Government or any agency thereof. The views and opinions of authors expressed herein do not necessarily state or reflect those of the United States Government or any agency thereof.

Metals and Ceramics Division

**MICROMECHANISMS OF DEFORMATION AND FRACTURE IN ORDERED
INTERMETALLIC ALLOYS - I. STRENGTHENING MECHANISMS**

M. H. Yoo, J. A. Horton, and C. T. Liu

Date Published: July 1988

Prepared for the
Office of Basic Energy Sciences
KC 02 01 05 0

Prepared by the
OAK RIDGE NATIONAL LABORATORY
Oak Ridge, Tennessee 37831
operated by
MARTIN MARIETTA ENERGY SYSTEMS, INC.
for the
U.S. DEPARTMENT OF ENERGY
under Contract DE-AC05-84OR21400

MARTIN MARIETTA ENERGY SYSTEMS LIBRARIES



3 4456 0280323 2

CONTENTS

ABSTRACT	1
I. INTRODUCTION	1
2. ACTIVE SLIP SYSTEMS	3
2.1 $L1_2$ STRUCTURE	5
2.1.1 Low and Intermediate Temperatures	5
2.1.2 High Temperatures	10
2.2 $B2$ STRUCTURE	12
2.2.1 Low and Intermediate Temperatures	12
2.2.2 High Temperatures	20
2.3 DO_3 AND $L2_1$ STRUCTURES	20
2.4 NONCUBIC STRUCTURES	21
3. TWIN MODES	22
3.1 CUBIC STRUCTURES	22
3.2 TETRAGONAL AND HEXAGONAL STRUCTURES	24
4. STRENGTHENING MECHANISMS	26
4.1 INTRINSIC EFFECTS	27
4.1.1 Anisotropy of APB Energy	27
4.1.2 Interaction Torque	29
4.1.3 Dislocation Core Transformation	30
4.1.4 Yield Stress	32
4.2 EFFECTS OF NONSTOICHIOMETRY AND ALLOYING	36
5. DISCUSSION	38
5.1 ANOMALOUS YIELD STRENGTH	38
5.2 STRAIN RATE EFFECTS	40
5.3 ORDER TWINNING	40
5.4 ALLOY HARDENING	41
5.5 DISLOCATION MOBILITY	41
6. SUMMARY	42
ACKNOWLEDGMENTS	42
REFERENCES	43

MICROMECHANISMS OF DEFORMATION AND FRACTURE IN
ORDERED INTERMETALLIC ALLOYS - I. STRENGTHENING MECHANISMS*

M. H. Yoo, J. A. Horton, and C. T. Liu

ABSTRACT

The stability and mobility of active slip and twin modes in superlattice structures, for both cubic and noncubic crystals, are theoretically investigated based on the energetics and kinetics of dislocation dissociations. The main concept of the force couplet model for the positive temperature dependence of yield and flow stresses is introduced. Two sources of the glide resistance in ordered lattices are the fault dragging mechanism and the cross-slip pinning mechanism. The effective fault energy consists of two terms related to the chemical and mechanical instability of a shear fault (antiphase boundary, superlattice intrinsic stacking fault, or microtwin). Dependence of the yield stress on the orientation and the sense of applied stress stems from the signs and magnitudes of the glide and nonglide stresses. As the effective fault energy is altered by solute segregation and/or high nonglide stress, the two glide resistance mechanisms are affected differently. In Ni₃Al and β -CuZn, the major aspects of anomalous yield strength, strain rate sensitivity, in situ deformation transmission electron microscopy observations, microtwinning, and nonstoichiometry effect are discussed in view of the present model. In addition, the order twinning-slip conjugate relationship is identified, in all the superlattice structures considered, which will influence the deformation behavior by viscous glide at high temperatures.

1. INTRODUCTION

Ordered intermetallic compounds have long been recognized for their superior strength at elevated temperatures. The strong tendency for chemical ordering in these intermetallic compounds reduces the atomic mobility at elevated temperatures and results in good structural stability

*Research sponsored by the Division of Materials Sciences, U.S. Department of Energy, under contract DE-AC05-84OR21400 with Martin Marietta Energy Systems, Inc.

A condensed version of this report, "Micromechanisms of Yield and Flow in Ordered Intermetallic Alloys," is to appear in *Acta Metall.* 36 (1988).

and resistance to high temperature deformation. However, the low symmetry crystal structures common to these materials give rise to poor ductility. Thus, strength and weakness coexist in ordered intermetallic compounds.

Much attention has been given to Ni_3Al with the L1_2 structure because of its unique deformation and fracture characteristics, viz., the anomalous (positive) temperature dependence of yield and flow stresses and the inherent susceptibility to intergranular fracture. The current status of our mechanistic understanding of both the anomalous yield strength and the inherently brittle grain boundary weakness in L1_2 ordered alloys can be assessed with the proceedings of two recent symposia.^{1,2} Though there have been significant advances recently, most theoretical analyses were made on the energetic basis alone and nearly all transmission electron microscopy (TEM) experiments to confirm operative mechanisms were performed statically after the mechanical testings. More recently, a stability analysis of superdislocations and shear faults in the L1_2 structure³ and in situ deformation TEM experiments on Ni_3Al (refs. 4,5) have been made. These investigations have disclosed several conclusions which cannot be accounted for by the prevailing theories available for the anomalous yield strength in L1_2 alloys.

Another outstanding example of anomalous yield behavior is $\beta\text{-CuZn}$ with the B2 structure. In this case also, there has been a number of in situ deformation high-voltage electron microscopy (HVEM) experiments to characterize dislocation behavior and mobility at various temperatures.⁶⁻⁸ Whereas much information on the multiplication process and the mobility of dislocations has been obtained, the major driving force for the anomalous yield behavior has not been identified. Also, it is not understood why only $\beta\text{-CuZn}$ and FeCo show the strength anomaly among B2 alloys. While Ni_3Al and $\beta\text{-CuZn}$ are the outstanding cases as far as the anomalous yield strength is concerned,⁹ a comprehensive analysis on a wide range of ordered intermetallics is deemed necessary in order to understand the micromechanisms of yield and flow behavior of this class of materials.

The purpose of this report is to analyze the deformation modes in superlattice structures, of both cubic and noncubic symmetries, on the basis of energetics and kinetics of dislocation dissociations, and to discuss possible micromechanisms for the temperature and strain rate dependencies of yield and flow stress in ordered intermetallic alloys. A systematic analysis will be made on the basis of the crystal symmetry, anisotropic elasticity, dislocation dynamics, and crystallography of twinning. In Sect. 2, the relative stability and mobility of superdislocations are assessed in terms of the change in their dissociation configurations. Interrelationships between the active slip system and "order-twinning" are established in Sect. 3. The physical sources for the temperature dependence and the strain rate sensitivity of yield and flow stresses are discussed in Sect. 4. Section 5 addresses the key issues in strengthening mechanisms, followed by a summary in Sect. 6.

2. ACTIVE SLIP SYSTEMS

Active slip systems reported in the literature^{10,11} are summarized in Table 1, where the slip vectors are Burgers vectors of superdislocations, \underline{B} . The Miller-Bravis indices for slip systems, $\{hk\cdot l\}\langle uv\cdot w\rangle$, in an ordered crystal structure are referred to the crystal structure of the corresponding disordered state (fcc for $L1_2$, $L1_0$, and DO_{22} ; bcc for $B2$, DO_3 , and $L2_1$; and hcp for DO_{19}). Some of those alloys which show the anomalous temperature dependence of yield stress are given in the last column.¹²⁻¹⁴ The elastic constants, C_{11} , C_{12} , and C_{44} , for cubic ordered alloys at room temperature¹⁵ are listed in Table 2 together with the anisotropy factors, A and R , relevant to the screw orientations $\langle 110 \rangle$ and $\langle 111 \rangle$ for the $L1_2$ and $B2$ (DO_3) structures,⁹ respectively.

Table 1. Observed slip systems in ordered intermetallic alloys

Crystal structure		Slip system		Anomalous strength
Cubic	L1 ₂	{111}, {010}	$\langle \bar{1}01 \rangle$	Cu ₃ Au, Co ₃ Ti, Pt ₃ Ti, Fe ₃ Ga (Fe, Co, Ni) ₃ V, Ni ₃ X (X = Al, Ga, Si, Ge)
Cubic	L2 ₀ (B2)	{ $\bar{1}\bar{1}0$ }, {11 $\bar{2}$ }, {12 $\bar{3}$ } { $\bar{1}\bar{1}0$ }	$\langle 111 \rangle$ $\langle 001 \rangle$	β -CuZn, FeCo
Cubic	DO ₃	{ $\bar{1}\bar{1}0$ }, {11 $\bar{2}$ }, {12 $\bar{3}$ }	$\langle 111 \rangle$	Fe ₃ Al, Fe ₃ Be*
Cubic	L2 ₁	{ $\bar{1}\bar{1}0$ }, {11 $\bar{2}$ } { $\bar{1}\bar{1}0$ }	$\langle 111 \rangle$ $\langle 110 \rangle, \langle 001 \rangle$	Ag ₂ MgZn
Tetragonal	L1 ₀	{111}	$\langle \bar{1}\bar{1}0 \rangle$ $\langle 0\bar{1}1 \rangle$	TiAl
Tetragonal	DO ₂₂	(001)	$\langle 110 \rangle$ $\langle 100 \rangle$	Ni ₃ V
Hexagonal	DO ₁₉	(0001), { $\bar{1}\bar{1}00$ }, {1 $\bar{1}01$ } {10 $\bar{1}1$ }, {11 $\bar{2}2$ }	$\langle 11\bar{2}0 \rangle$ $\langle 11\bar{2}3 \rangle$	Mg ₃ Cd, Mn ₃ Sn

*Pseudotwinning is the deformation mode.

Table 2. Elastic constants of ordered cubic intermetallic alloys at room temperature

Type	Alloy	10 ¹¹ N/m ² .			A	R	Ref. 15
		C ₁₁	C ₁₂	C ₄₄			
L1 ₂	Ni ₃ Al	2.23	1.48	1.25	3.34	1.12	a, m
	Ni ₃ Fe	2.46	1.48	1.24	2.53	1.07	b
	Cu ₃ Au	1.87	1.35	0.68	2.60	1.08	c
DO ₃	Fe ₃ Si	2.32	1.56	1.35	3.59	1.13	k
	Fe ₃ Al	1.72	1.32	1.32	6.52	1.30	d
B2	FeAl*	2.09	1.23	1.27	2.94	1.09	d
	NiAl	2.12	1.43	1.12	3.28	1.12	e
	AgMg	0.84	0.56	0.48	3.47	1.13	f, l
	CuZn(II)	1.34	1.04	0.73	4.94	1.23	g
	CuZn(I)	1.29	1.10	0.82	8.49	1.43	h
	AuZn	0.50	0.38	0.37	5.92	1.27	i
	AuCd	0.90	0.83	0.44	11.86	1.64	j

*Extrapolated from the lower Al concentrations.

2.1 L1₂ STRUCTURE

2.1.1 Low and Intermediate Temperatures*

Consider a single dislocation loop of Burgers vector, $\underline{B} = [\bar{1}01]$, lying in a (111) plane dissociated according to the antiphase boundary (APB)-type dissociation

$$\underline{B} \rightarrow \underline{b} + \underline{b} , \quad (1)$$

where $\underline{b} = \frac{1}{2}[\bar{1}01]$ (Fig. 2). The interaction force between the two superpartial dislocations was calculated earlier by using anisotropic elasticity theory.³ The orientation dependence of the radial and tangential components for the (111) APB-type dissociation in Ni₃Al is shown in Fig. 3. For the screw orientation ($\phi = 0^\circ$), the strength ratio of the tangential component to the radial component is $f_1 = f_\theta/f_r = (A - 1)\sqrt{2}/(A + 2)$, where $A = 2C_{44}/(C_{11} - C_{12})$. According to the elastic constants listed in Table 2, $f_1 \approx 0.6$ for Ni₃Al, Cu₃Au, and Ni₃Fe. Figure 3 shows that this ratio increases with increasing ϕ to the maximum value of $f_1 \approx 0.7$ at $\phi = 31^\circ$, and then decreases to zero at the edge orientation ($\phi = 90^\circ$). The variation of f_r and f_θ with dislocation character is depicted schematically in Fig. 2.

Mobility of the edge component is expected to be much higher than that of the screw component for the following reasons:

1. The larger the dislocation width, the lower the Peierls stress.¹⁶⁻¹⁸ The extended width of a superdislocation is proportional to f_r , which is larger for the edge component than for the screw component (Fig. 3).
2. Similarly, for the core width of each superpartial, the mobility of the edge component is relatively higher.

*Low, intermediate, and high temperatures are referred to homologous temperatures below and above the peak temperature of anomalous yield strength, T_p , of Ni₃Al. See the three regions shown in Fig. 1.

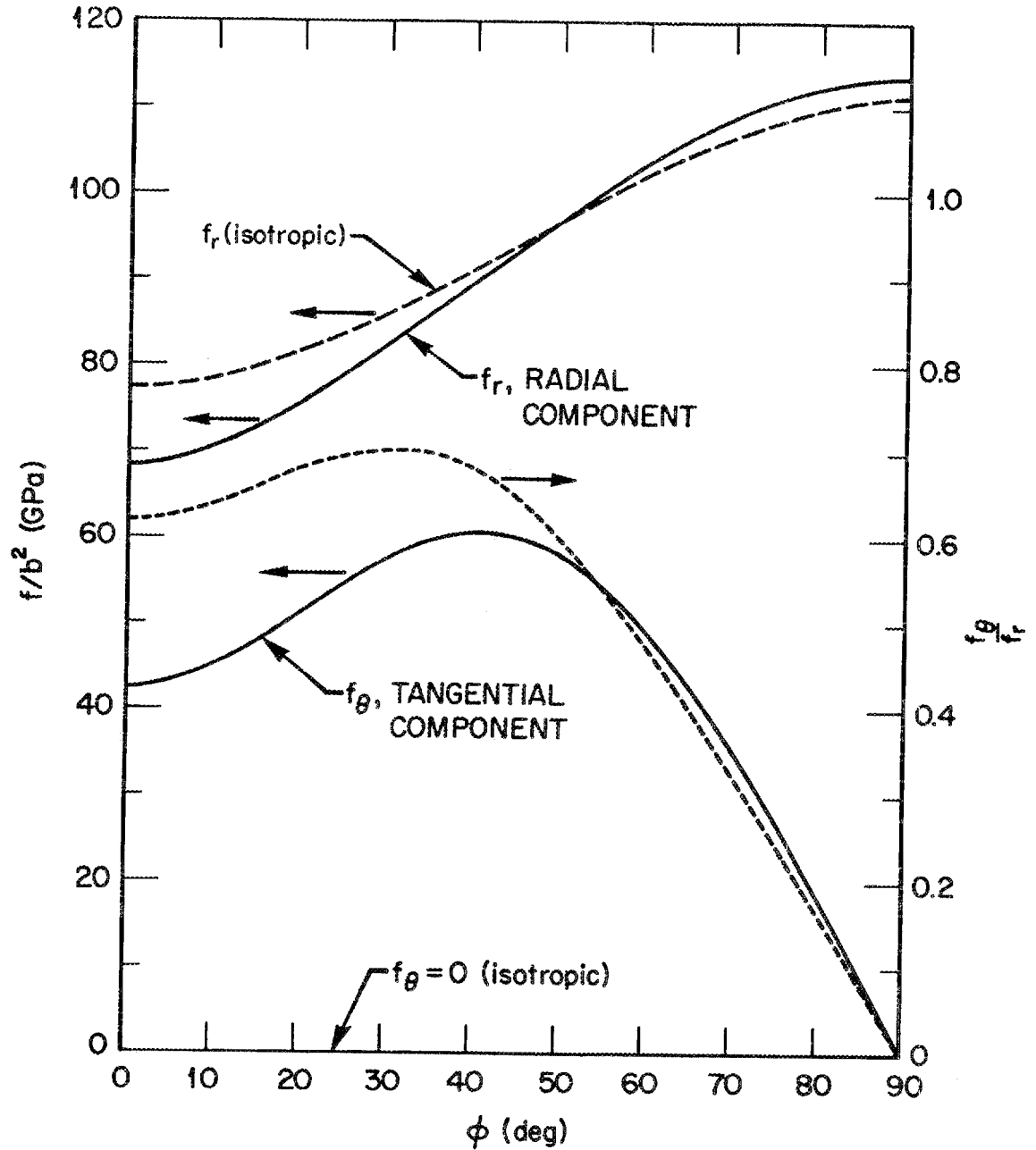


Fig. 3. Orientation dependences of the interaction force constants in Ni_3Al at room temperature for the (111) APB-type dissociation.

3. The effect of elastic anisotropy on the dislocation mobility is to further increase the disparity between the two dislocation characters (see the two f_r curves in Fig. 3).
4. For near-screw orientations, there may exist intrinsic resistance to dislocation motion due to a distribution of force couplets across the APB ribbon, Fig. 4(a), which is necessary to counterbalance the interaction torque between the two superpartials.^{3,9,19} As was mentioned in review articles,^{10,20} postdeformation TEM observations in $L1_2$ alloys showed primarily long straight screw dislocations. More convincing direct evidence for the strong disparity of dislocation mobility between the edge and screw components has been obtained recently in Ni_3Al by conducting an in situ deformation TEM experiment.⁵

The last point (No. 4) mentioned above is unique to the case of dislocation dissociations in a superlattice with long-range ordering (LRO). This can be discussed further with the aid of Fig. 4. The magnitudes of the interaction force components (Fig. 4) are $F_r = f_r/2\pi r$ and $F_\theta = f_\theta/2\pi r$, where f_r and f_θ are given in Fig. 3. Bending of the shear-type APB ribbon due to the force couplets, as depicted in Fig. 4(a), can be associated with a continuous distribution of fractional edge dislocation pairs (a twofold symmetry with respect to the z-axis) such that the fault vector, $\underline{f} = \underline{b} \pm \underline{b}'$, where $\underline{b} = \frac{1}{2}[\bar{1}01]$, $\underline{b}' = \frac{\chi}{6}[1\bar{2}1]$, and $0 < \chi < 1$. Figure 4(b) shows this dissociation configuration which is in a state of static equilibrium. When an externally applied stress, σ_a , is imposed onto this static configuration, the twofold symmetry of Fig. 4(b) will generally be destroyed as in the case of cross-slip pinning configuration⁹ shown in Fig. 4(e).

When a uniaxial applied stress, σ_a , is applied in a certain crystallographic direction of a crystal, the resolved shear stress, τ_{xy} , for the edge component, \underline{b}' , favors the stability of APB ribbon interface when $\tau_{xy} > 0$ and the nucleation of a superlattice intrinsic stacking

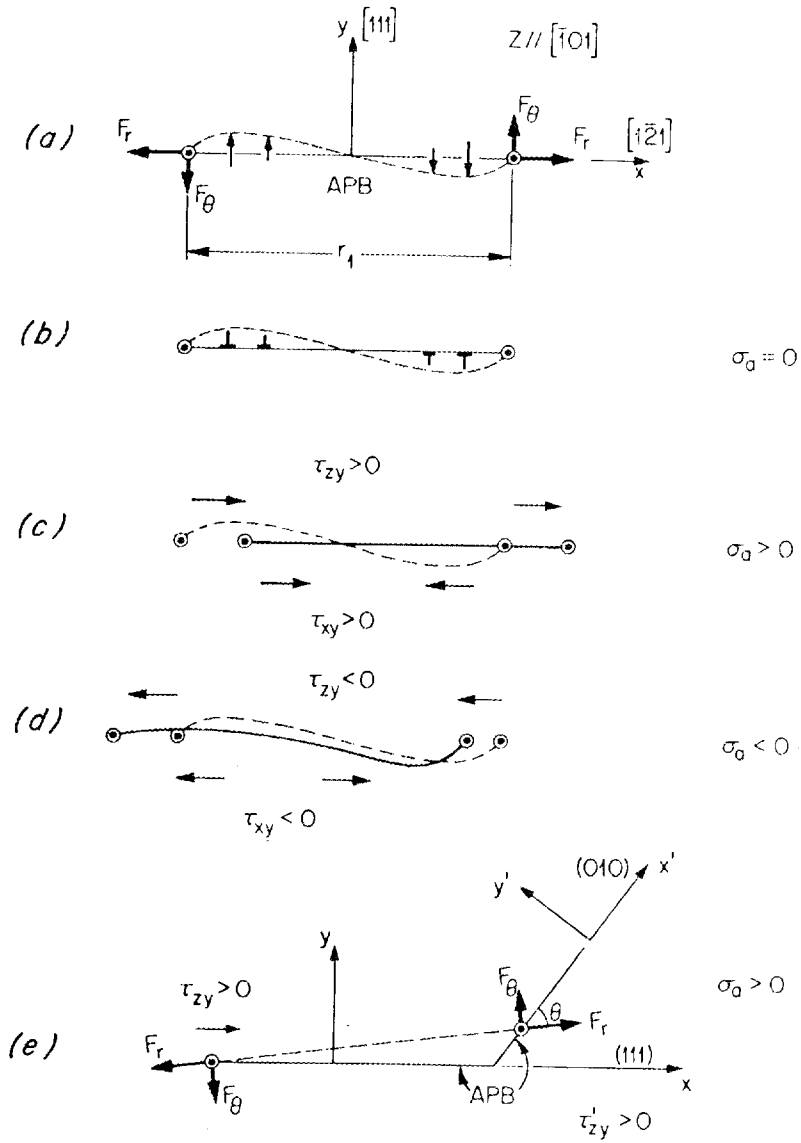


Fig. 4. Possible dissociation configurations of a screw superdislocation in the $L1_2$ structure; (a) force couplets, (b) fractional edge pairs, (c) stabilized APB, (d) stress-induced SISF, and (e) cross slip.

fault (SISF) when $\tau_{xy} < 0$. Under a tensile stress, σ_a , which resolves into $\tau_{zy} > 0$ and $\tau_{xy} > 0$,* as in Fig. 4(c), the bending of APB interface would tend to straighten out, and the mobility of the superdislocation will be enhanced. When the sign of σ_a is reversed, $\tau_{zy} < 0$ and $\tau_{xy} < 0$, the trailing superpartial will be impeded as shown in Fig. 4(d). If the constriction of Shockley partials is effected and the resolved shear stresses on both the primary and the cross-slip planes are sufficiently high, $\tau_{zy} > 0$ and $\tau'_{zy} > 0$, then a cross slip pinning configuration as shown in Fig. 4(e) is possible.^{9,19} In this case, the leading superpartial will be impeded.

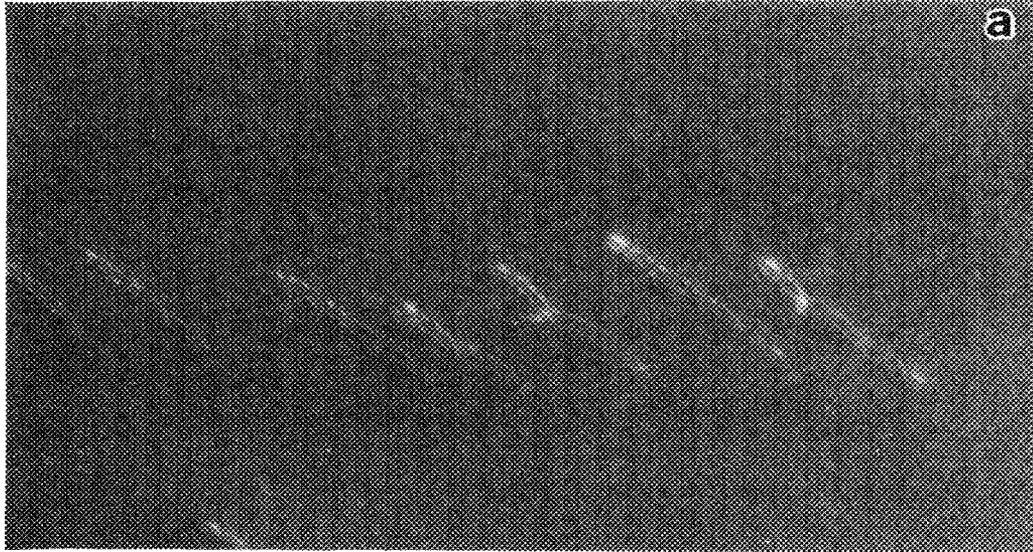
That all three dynamic configurations, Figs. 4(c), 4(d), and 4(e), are possible during deformation is corroborated by recent experimental findings.^{4,5} Figures 5(a) and 5(b) represent evidence for the cases of Figs. 4(c) and 4(d), respectively. A combination of the two cases, Figs. 4(c) and 4(e), could account for the direct observation made by Baker et al.⁴ All of these experiments were carried out at room temperature, and the separation spacing between the superpartials under an applied stress was found to be, in all cases, greater than the static equilibrium width, e.g., $r_1 = 6.7$ nm for the screw orientation.²³ These observations indicate that the configuration of the cross-slip pinning process, Fig. 4(e), is not solely responsible for the anomalous strengthening phenomenon.

2.1.2 High Temperatures

As the deformation temperature, T , is raised, the $\{010\}\langle\bar{1}01\rangle$ cross-slip system becomes gradually more active and becomes the primary slip system at $T > T_p$. The fact that the APB energy on $\{010\}$ planes is lower than that on $\{111\}$ planes^{9,24,25} and no interaction torque exists on $\{010\}$ planes^{3,19} would suggest a relatively high superdislocation

*In the case of bcc structure, Duesbery called τ_{zy} "glide stress" and τ_{xy} , "nonglide stress" or "edge stress" (refs. 21,22).

YP6060



YP6058



Fig. 5. Superpartial dislocations at the head of slip bands in Ni_3Al under load; (a) APB coupled superpartials, $\underline{b} = \frac{1}{2}[\bar{1}01]$, $r_1 \approx 7$ nm and (b) the leading superpartial trailing long SISFs, $\underline{b} = \frac{1}{3}[\bar{1}\bar{1}2]$.

mobility. However, computer simulation analyses of the core structure of screw superpartials^{26,27} showed two distinct atomic configurations, a glissile one on {111} planes and a sessile one on {010} planes. In the latter case, therefore, the mobility of the sessile core configuration seems to control the dynamic process of {010}< $\bar{1}01$ > slip. No direct experimental study of {010}< $\bar{1}01$ > slip has been done. Based on weak-beam TEM analysis, at room temperature, of superdislocations moved on {010} planes at 800°C in Ni₃Al, Veyssi re²⁸ envisaged nonplanar dissociation of a mixed dislocation by the glide-climb separation of the superpartial pair.

2.2 B2 STRUCTURE

2.2.1 Low and Intermediate Temperatures*

As shown in Table 1, several slip planes were identified with Burgers vector, $\underline{b} = m\langle 111 \rangle$, where $m = 1$ for B2 and $m = 2$ for DO₃ or L2₁ structures respectively.¹¹ In an analogous manner as for the bcc structure,²⁹ two possible ways of sessile splitting of the \underline{b} screw dislocation that maintain a threefold symmetry are shown in Figs. 6(a) and 6(b). The displacement component perpendicular to the $\langle 111 \rangle$ screw dislocation line, u_n , which arises due to the elastic anisotropy,³⁰ is shown in Fig. 7(a). The distribution of displacement vectors shown in Fig. 7(a) may be attributed to two sets of force triplets[†] oriented along $\langle 1\bar{1}0 \rangle$ directions, one set outward and the other inward with respect to the origin. This displacement field may be regarded as a bending of the originally cylindrical surface by a distribution of fractional edge dislocations as shown in Fig. 7(b).

* $T < T_p$. The reference peak temperature, in this case, is for β -CuZn (see Fig. 1 and Table 3).

[†]Because of a threefold symmetry with respect to the dislocation line, the term "triplet" is more appropriate than "doublet" used by Duesbery.²¹

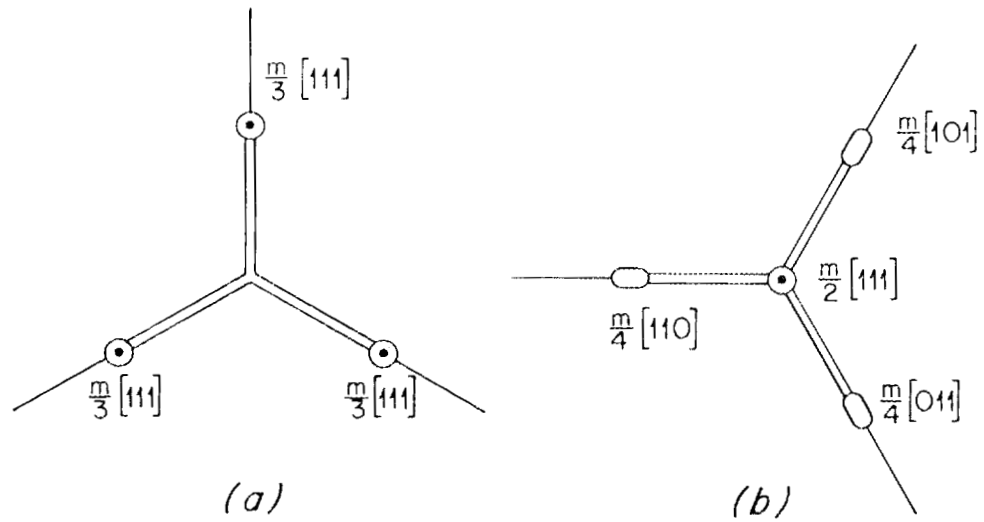


Fig. 6. Sessile splitting of an $m[111]$ screw superdislocation in the bcc-based superlattices on (a) $\{11\bar{2}\}$ planes and (b) $\{1\bar{1}0\}$ planes.

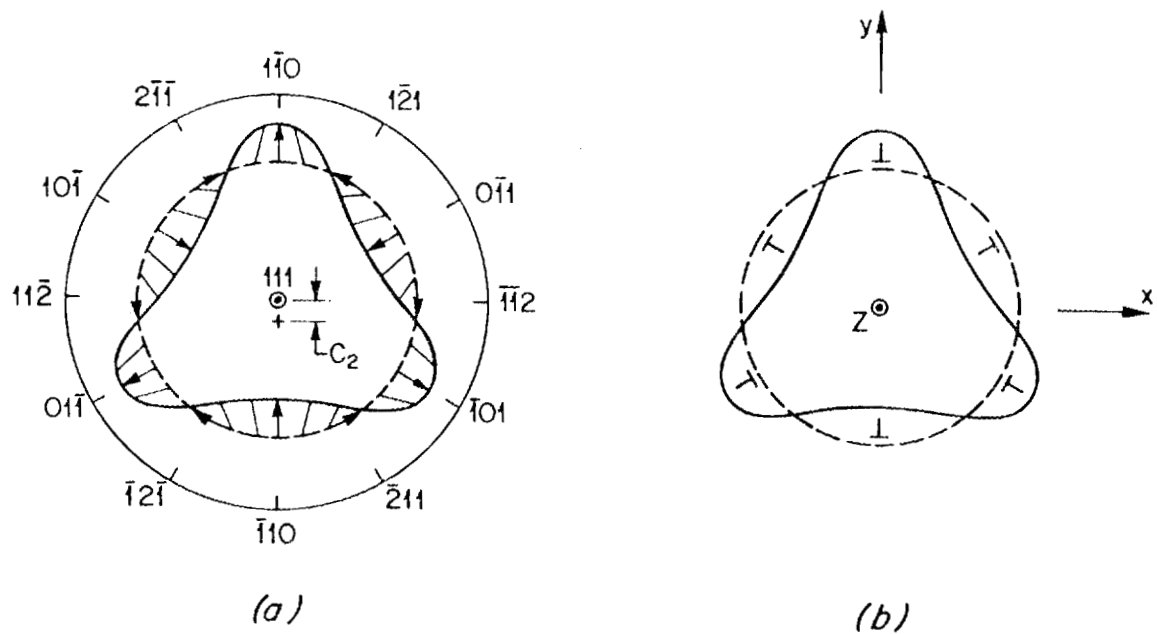


Fig. 7. The displacement component normal to a screw superdislocation, $\underline{B} = m[111]$, (a) distribution of displacement vectors and (b) distribution of fractional edge dislocations.

Table 3. Reference temperatures for the yield strength anomaly

Material	Temperature ^a (K)			
	T _b	T _p	T _c	T _m
Ni ₃ Al	~77	~1000	>1668	1668
β-CuZn	~300	~500	741	1143

^aT_c = the critical temperature for ordering, T_m = the melting point. See Fig. 1 for T_b and T_p.

In the case of CuZn(I) [ref. 15h], the maximum value of the normal displacement is $u_n \approx 0.03 B$ and the integration constant is $C_2 \approx -0.02 B$. The integration constant is generally required in order to determine the origin of the dislocation coordinate system with respect to the crystal axis for the dislocation.³⁰ When the integration constant is set to zero in Fig. 7(a), the displacement along the $[1\bar{1}0]$ direction is increased to $u_n = u_y \approx 0.05 B$, whereas the displacement along the $[01\bar{1}]$ or the $[\bar{1}01]$ direction is reduced to $u_n \approx u_x \approx \pm 0.03 B$, $u_y \approx 0$. If the physical significance of C_2 is that the screw dislocation of a threefold symmetry is elastically unstable and tends to contain a net edge component lying on the $(11\bar{2})$ plane, then a core transformation into an asymmetric splitting is possible on the $(11\bar{2})$ plane,

$$\underline{B} \rightarrow \underline{b}_1 + \underline{b}_2, \quad (2)$$

where $\underline{b}_2 > \underline{b}_1$ and \underline{b}_2 is situated toward the $[1\bar{1}0]$ direction as in the screw orientation of Fig. 8(b). Although the magnitude of u_n is rather small compared to that of \underline{B} , the residue of u_n offers important information on the relative measure of the asymmetric distribution of \underline{B} as well as the specific habit plane of asymmetric dissociation.

Since $\underline{b} = \frac{1}{2}\langle 111 \rangle$ is the fault vector for an APB in the B2 structure,¹¹ a dissociation of the type represented by Eq. (1) is

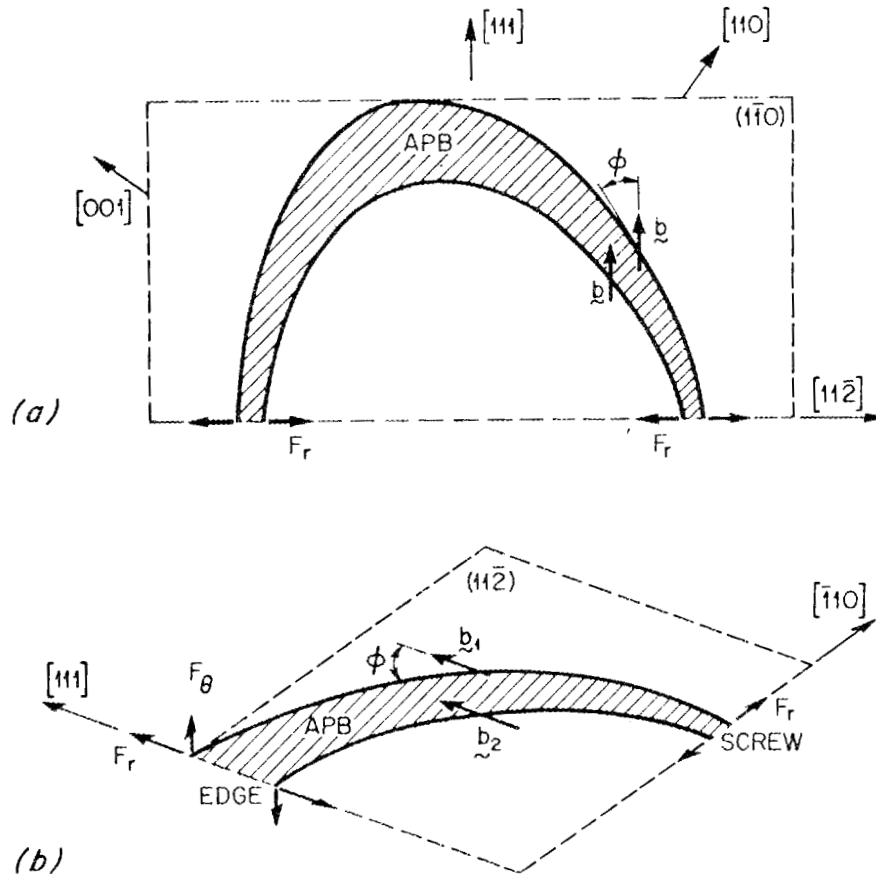


Fig. 8. The APB-type dissociations of $\underline{B} = [111]$ in the B2 structure on (a) the $(1\bar{1}0)$ plane and (b) the $(11\bar{2})$ plane.

expected to occur on a (hkl) plane which is cozonal to the $[111]$ axis, such as $(1\bar{1}0)$ and $(11\bar{2})$ planes. Single dislocation loops dissociated in the $(1\bar{1}0)$ and $(11\bar{2})$ planes are depicted in Figs. 8(a) and 8(b), respectively. These schematic diagrams were sketched based on the interaction forces between the superpartials with $\underline{b} = \frac{1}{2}[111]$ that were calculated with anisotropic elasticity theory (see Fig. 9). It should be noted in Fig. 9 that the effect of elastic anisotropy on f_r is much more pronounced in the B2 structure than the corresponding effect in the $L1_2$ structure (Fig. 3). This means that the disparity of dislocation mobility, viz., the $\frac{1}{2}\langle 111 \rangle$ screw dislocation is relatively immobile and

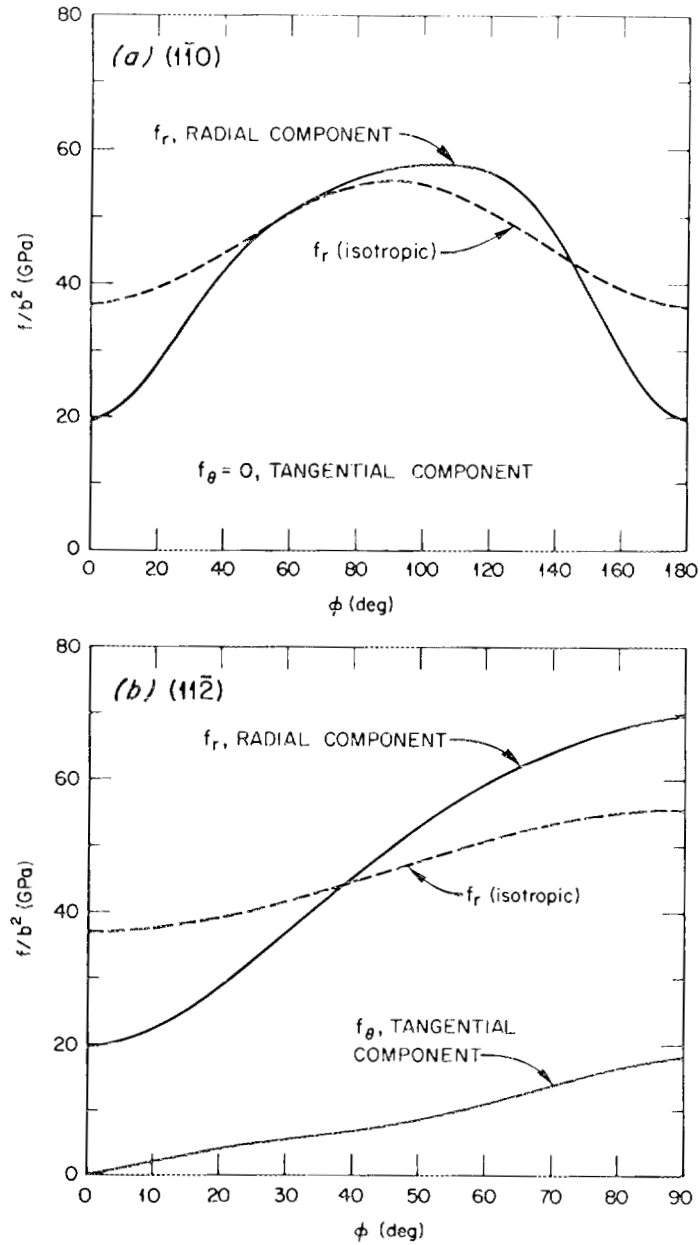


Fig. 9. Orientation dependences of the interaction force constants in β -CuZn at room temperature for the APB dissociation with $\underline{b} = \frac{1}{2}[111]$ on (a) the $(1\bar{1}0)$ plane and (b) the $(11\bar{2})$ plane.

is further enhanced by the elastic anisotropy effect. Because of a twofold symmetry of the slip-plane normal, $[1\bar{1}0]$, no tangential interaction force exists on the $(1\bar{1}0)$ plane at any orientation of the dislocation character as in Fig. 9(a). In the $(11\bar{2})$ plane, however, interaction torque arises at nonscrew orientations as shown in Fig. 9(b). Using the elastic constants of CuZn(I) given in Table 2, we find the maximum ratio of F_{θ}/F_r at the edge orientation ($\phi = 90^\circ$) to be 0.26.

In a similar manner as in Fig. 4, bending of the $(11\bar{2})$ APB interface can be related to a continuous distribution of fractional edge partial pairs, as in Figs. 10(a) and 10(b). Since the fault vector in this case is $\underline{f} = \underline{b} \pm \underline{b}'$, where $\underline{b} = \frac{1}{2}[111]$, $\underline{b}' = \frac{\chi'}{6}[111]$, and $0 < \chi' < 1$, the net distribution of the Burgers vector of an edge superdislocation on an $(11\bar{2})$ plane is asymmetric in accordance with Eq. (2), where \underline{b}_1 ($\underline{b}_1 < \underline{b}_2$) is situated toward the $[111]$ direction. This asymmetric dissociation for edge orientation is consistent with the prediction for the screw orientation discussed above. An overall picture of the asymmetric dissociation of a superdislocation pair situated in an $(11\bar{2})$ plane is shown in Fig. 8(b).

When the resolved shear stress is positive, $\tau_{xy} > 0$ in Fig. 10(c), the originally bent APB tends to straighten out, hence the APB will be stabilized, the equilibrium spacing, r_2 , will be essentially unchanged, and the mobility of the dissociated configuration will be enhanced. Upon reversing the sign of applied stress, $\tau_{xy} < 0$ in Fig. 10(d), which causes the pair shown in Fig. 8(b) to expand, the disparity of $b_2 > b_1$ will increase, and the trailing superpartial, \underline{b}_1 , will be impeded. If $\chi' = 1$ and $\underline{b}' = \frac{1}{6}[111]$ such that $\underline{b}_2 = \frac{2}{3}[111]$ and $\underline{b}_1 = \frac{1}{3}[111]$, a passage of the dissociated configuration as depicted in Fig. 11(d) is equivalent to "order twinning" by the leading \underline{b}_2 and a partial detwinning by the trailing \underline{b}_1 . This will be discussed further in Sect. 3. Finally, the interaction torque promotes the climb dissociation of the superpartial pair as shown in Fig. 10(e). This causes nonconservative motion of the APB interface which is more feasible under a high resolved normal stress, $\sigma_x > 0$, and at elevated temperatures.

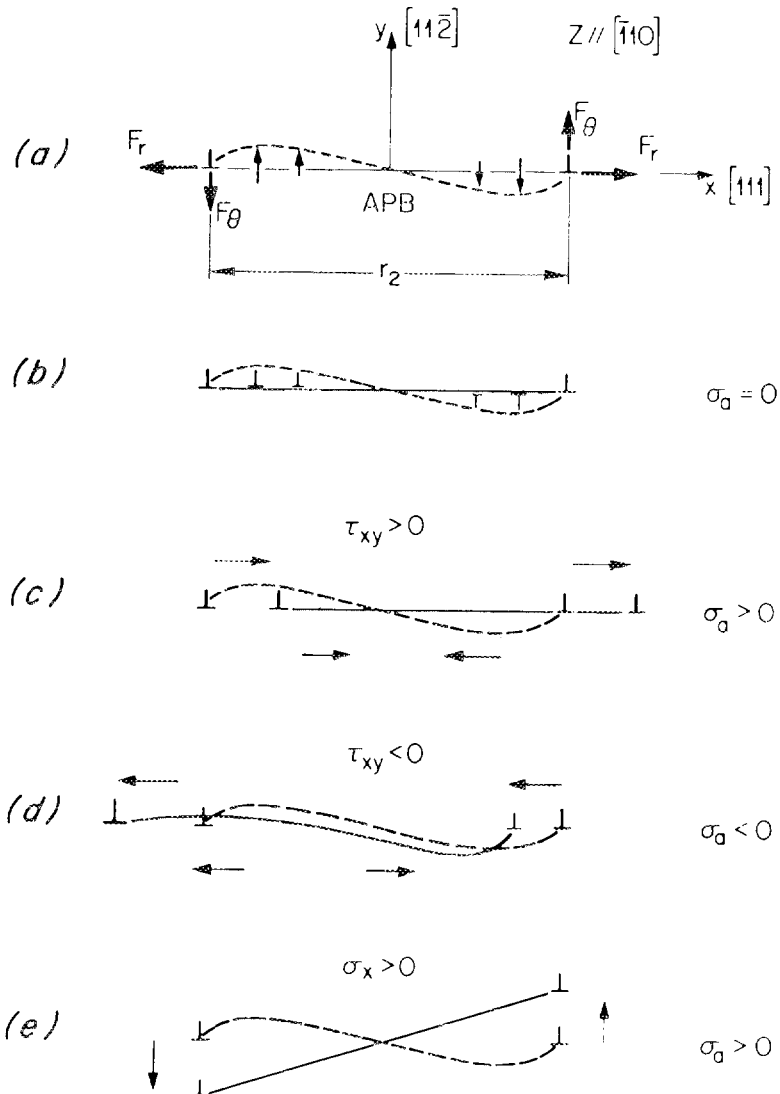


Fig. 10. Possible dissociation configurations of a $(11\bar{2})[111]$ edge superdislocation in the B2 structure; (a) force couplets, (b) fractional edge pairs, (c) stabilized APB, (d) order twinning, and (e) climb dissociation.

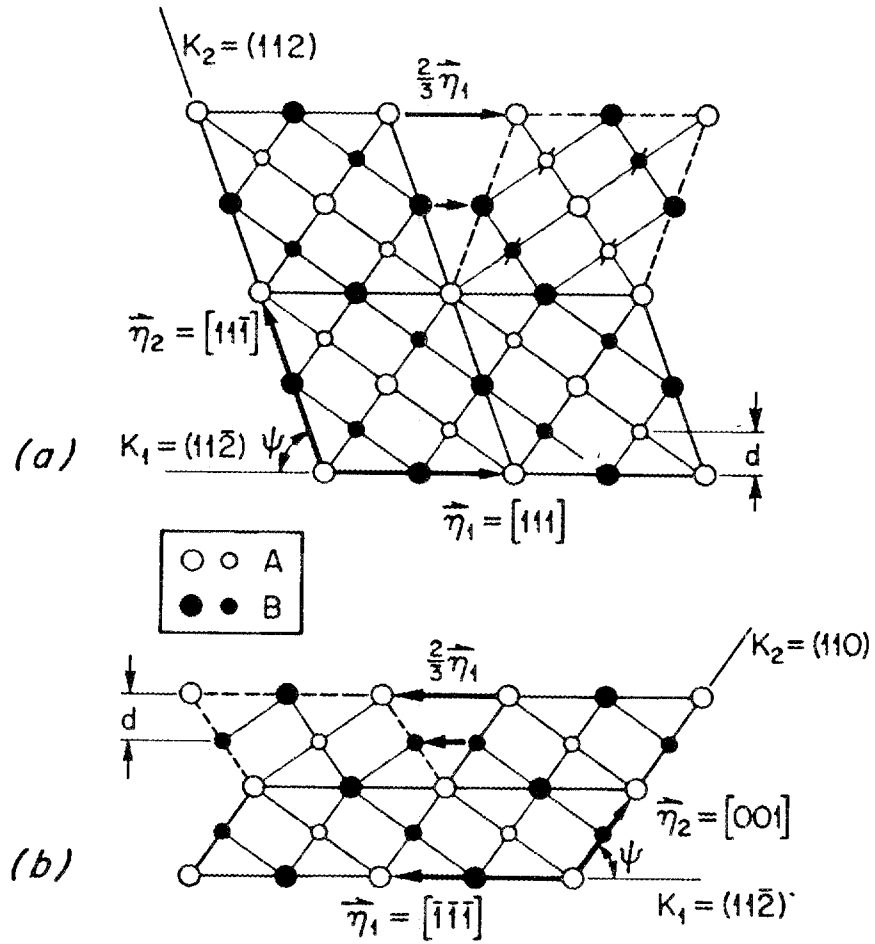


Fig. 11. Crystallographic elements of (a) bcc twinning, $\psi = 70.53^\circ$; and (b) order twinning, $\psi = 54.74^\circ$, in the B2 structure (AB).

2.2.2 High Temperatures

The dissociation of $\underline{B} = \langle 111 \rangle$ superdislocations in β -CuZn deformed at 190°C was examined by Saka and Zhu³¹ with the use of the weak-beam TEM technique. They found that the two superpartials, Eq. (1) and Fig. 8(a), were climb-dissociated both in edge and near screw orientations.

With increasing deformation temperature, a transition of active slip vector has been known to occur, from $\langle 111 \rangle$ to $\langle 110 \rangle$ and $\langle 001 \rangle$, in the B2 structure.^{11,32-35} One possible mechanism for this transition is the following reaction on an $(\bar{1}\bar{1}0)$ plane:



$\underline{B} = [111]$, $\underline{B}_1 = [001]$, and $\underline{B}_2 = [110]$. At the orientation $[110]$ or $[100]$ indicated in Fig. 8(a), the total Burgers vector \underline{B} of mixed character ($\phi = 35.3^\circ$ or 125.3°) may decompose into \underline{B}_1 and \underline{B}_2 , which are of either pure edge or screw character. Since there is no net change in the anisotropic elastic energy, the reaction, Eq. (3), is statically indeterminate. According to the line tension analyses of a superdislocation loop,^{3,36,37} it is negative in β -CuZn at either orientation. Therefore, the dislocation reaction, Eq. (3), can occur spontaneously because of the instability of elastic line tension of a total dislocation loop.

2.3 DO₃ AND L2₁ STRUCTURES

The discussion given in Sect. 2.2 is generally pertinent to the DO₃ and L2₁ (Heusler) structures with $\underline{B} = 2[111]$. Figures 6 and 7 are directly applicable here with $m = 2$. In addition to the twofold dissociation of \underline{B} , Eq. (1) and Fig. 8(a) or Eq. (2) and Fig. 8(b), a fourfold dissociation is also possible in the DO₃ and L2₁ structures,



where $\underline{b} = \frac{1}{2}[111] \pm \underline{b}'$ and the magnitude and direction of \underline{b}' may vary from material to material.¹¹ The fourfold dissociation in a DO_3 -ordered Fe-26 at. % Al alloy investigated by weak-beam TEM analysis³⁸ is consistent with Eq. (4) and $\underline{b}' = 0$ since there is no interaction torque between the dislocations lying on an $(1\bar{1}0)$ plane. When the dissociation occurs on an $(11\bar{2})$ plane, the fractional Burgers vector is $\underline{b}' = \frac{\chi}{6}[111]$.

Both $\underline{B} = \langle 110 \rangle$ and $\underline{B} = \langle 001 \rangle$ are possible slip vectors in $L2_1$ alloys at elevated temperatures.³⁹ The proposed mechanism for the B2 structure, Eq. (3), may be also applicable here for the $L2_1$ structure. In the Al-rich Ni_2AlTi alloy, a twofold dissociation, Eq. (1), of $\underline{B} = \langle 001 \rangle$ and $\underline{b} = \frac{1}{2}\langle 001 \rangle$ on $\{110\}$ planes was observed by TEM analysis,⁴⁰ which is consistent with the fact that $\underline{b}' = 0$ on twofold symmetry $\{110\}$ planes.

2.4 NONCUBIC STRUCTURES

In both $L1_0$ and DO_{22} tetragonal structures,⁴¹⁻⁴⁴ the slip activity is mainly propagation of partial dislocations bounding pure stacking fault without any wrong nearest neighbor bonds and results in a profuse microtwinning. At elevated temperatures, slips of the types $\underline{B} = [110]$, $[100]$, and $[010]$ becomes operative in the DO_{22} structure.⁴⁵

In the hexagonal DO_{19} structure, slip systems of $\underline{B} = \frac{2}{3}\langle 11\bar{2}0 \rangle$ on the basal (0001) and nonbasal $\{1\bar{1}00\}$ and $\{1\bar{1}01\}$ planes are active at low temperatures.^{13,20} Dislocation pairs of like sign, $\underline{b} = \frac{1}{3}\langle 11\bar{2}0 \rangle$, have been observed by TEM in all of the above slip systems.²⁰ At elevated temperatures, nonbasal slip systems of $\underline{B} = \frac{2}{3}\langle 11\bar{2}\bar{3} \rangle$ on $\{10\bar{1}1\}$ and $\{11\bar{2}2\}$ planes are operative. The interaction torque between a pair of dislocations in this case was computed earlier.⁴⁶ As will be discussed later (Sect. 4), the interaction torque between a pair of screw dislocations of $\underline{b} = \frac{1}{3}[11\bar{2}0]$ is zero on the basal and prism planes and nonzero on a pyramidal plane. Therefore, in the case of a primary slip system of $\{1\bar{1}01\}\langle 11\bar{2}0 \rangle$ in Mg_3Cd at room temperature,²⁰ the interaction torque plays a role similar to the $\{111\}\langle 10\bar{1} \rangle$ in Ni_3Al .

3. TWIN MODES

3.1 CUBIC STRUCTURES

The crystallography of twinning in cubic superlattices has been discussed earlier.^{20, 47-49} Table 4 shows the crystallographic elements ($K_1, K_2, \vec{\eta}_1, \vec{\eta}_2$) and parameters (q, g) for cubic ordered structures. The \vec{s} is the normal to the plane of shear, g is the twinning shear, and q is an integer such that some atomic shuffling is necessary when $q > 2$ (ref. 47). In Figs. 11 and 12, the open circles are A atoms, the filled circles are B atoms, the larger circles represent atoms in the plane of projection, and the smaller circles represent those in the adjacent planes. In the $L1_2$ and B2 structures, the primary twin system ($K_1, \vec{\eta}_1$) requires atomic shuffling on every other twin plane as indicated by the stokes on circular symbols in Fig. 11(a) for the case of B2 structure. This means that the mobility of twinning dislocations would be extremely low.⁴⁷ In the complementary twin system, g is twice as large as in the primary twin system, but no atomic shuffling is necessary, as shown in Fig. 11(b).

Table 4. Crystallographic elements and parameters of twin modes in cubic ordered structures

Structure type	Twin system ^a	K_1	K_2	$\vec{\eta}_1$	$\vec{\eta}_2$	\vec{s}	q	g
$L1_2$	P	$\{111\}$	$\{\bar{1}\bar{1}\bar{1}\}$	$\langle\bar{1}21\rangle$	$\langle121\rangle$	$\langle\bar{1}01\rangle$	4	$1/\sqrt{2}$
	C	$\{111\}$	$\{010\}$	$\langle\bar{1}2\bar{1}\rangle$	$\langle101\rangle$	$\langle10\bar{1}\rangle$	2	$\sqrt{2}$
B2	P	$\{11\bar{2}\}$	$\{112\}$	$\langle\bar{1}11\rangle$	$\langle11\bar{1}\rangle$	$\langle\bar{1}10\rangle$	4	$1/\sqrt{2}$
	C	$\{11\bar{2}\}$	$\{110\}$	$\langle\bar{1}11\rangle$	$\langle001\rangle$	$\langle\bar{1}10\rangle$	2	$\sqrt{2}$
$DO_3, L2_1$	P	$\{11\bar{2}\}$	$\{112\}$	$2\langle\bar{1}11\rangle$	$2\langle11\bar{1}\rangle$	$2\langle\bar{1}10\rangle$	8	$1/\sqrt{2}$
	C	$\{11\bar{2}\}$	$\{110\}$	$2\langle\bar{1}11\rangle$	$2\langle001\rangle$	$2\langle\bar{1}10\rangle$	4	$\sqrt{2}$

^aP = primary, C = complementary.

ORNL-DWG 87-11187

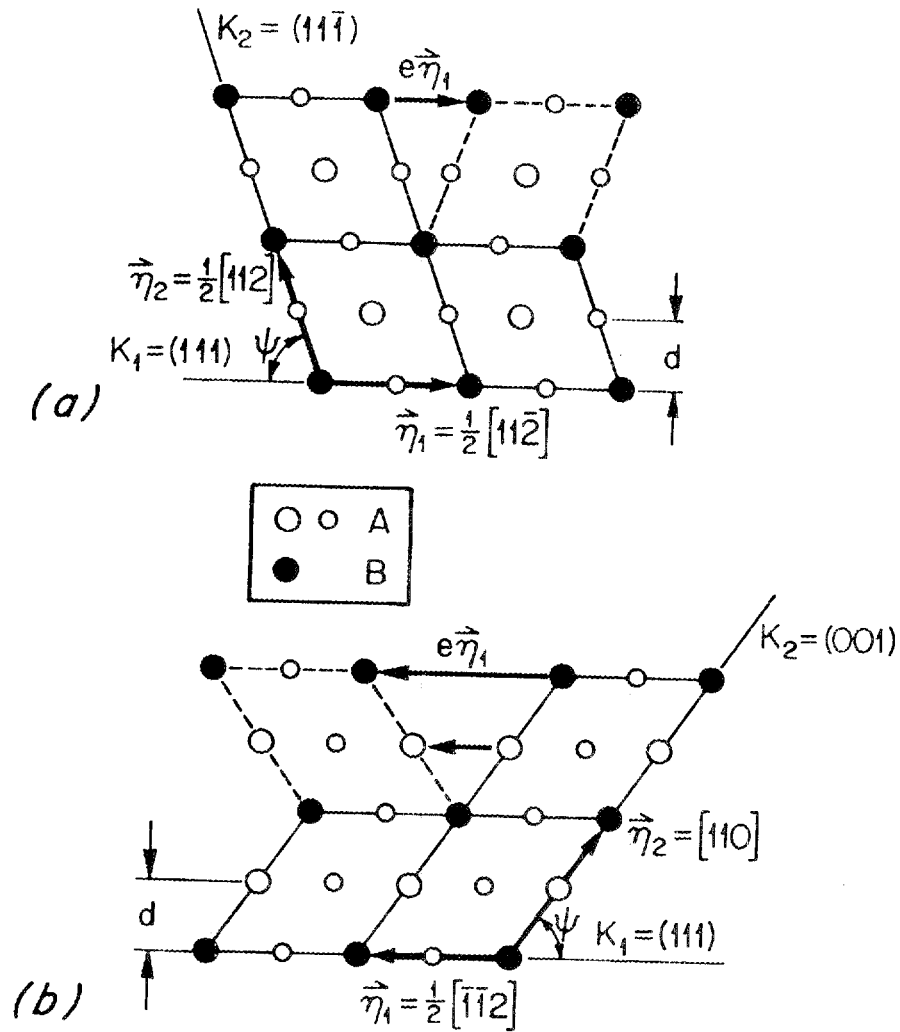


Fig. 12. Crystallographic elements of (a) primary twinning and (b) complementary twinning in the $D0_{22}$ structure (A_3B). The drawing is based on $c/a = 1$.

Therefore, in fully ordered $L1_2$ and B2 alloys, the complementary twinning, also called "order-twinning" or "super-twinning" (ref. 50), is much more feasible than the primary twinning which is also called fcc- or bcc-twinning.

In the $L2_1$ structure, pseudotwinning arises from the interaction of LRO and twinning. The increase in ordering energy associated with the phase transition may give rise to a restoring force responsible for the reversion of the pseudotwin in Fe_3Be upon unloading. This phenomenon will be analyzed elsewhere.⁵¹

It is important to recognize the fact that, in all cases, the conjugate deformation mode to order-twinning is the secondary slip system, which becomes the primary slip system at high temperatures, viz., $\{010\}\langle 101\rangle$ for the $L1_2$ structure and $\{110\}\langle 001\rangle$ for the B2 and the related structures. This implies that macrotwinning will be feasible when the accommodation slip by the secondary slip system is enhanced. Conversely, when the conjugate slip system becomes active at high temperatures, the primary strengthening mechanism will be related to microtwinning.

3.2 TETRAGONAL AND HEXAGONAL STRUCTURES

Concerning the geometrical requirements for general polycrystalline deformation, twinning plays a relatively more important role in materials of noncubic crystal structures than of cubic structures. However, the energetic and kinetic aspects of twinning in noncubic ordered structures are not well understood. We will defer detailed discussions⁵¹ and treat here only briefly tetragonal $L1_0$ and DO_{22} structures and hexagonal DO_{19} structure that are crystallographically related to the $L1_2$ structure.

It should also be noted that in the tetragonal structure, Fig. 13, the conjugate deformation mode to the complementary twin system is the active slip system. However, in this case, even the primary twin system does not require atomic shuffling, $q = 2$ or 1 (see Fig. 12). The drawing in Fig. 12 is for the DO_{22} structure, but it is also applicable for the $L1_0$ structure when the larger open circles are changed to large filled circles. The twinning shear of the primary twin system is considerably smaller than that of the complementary twin system. Therefore, from the

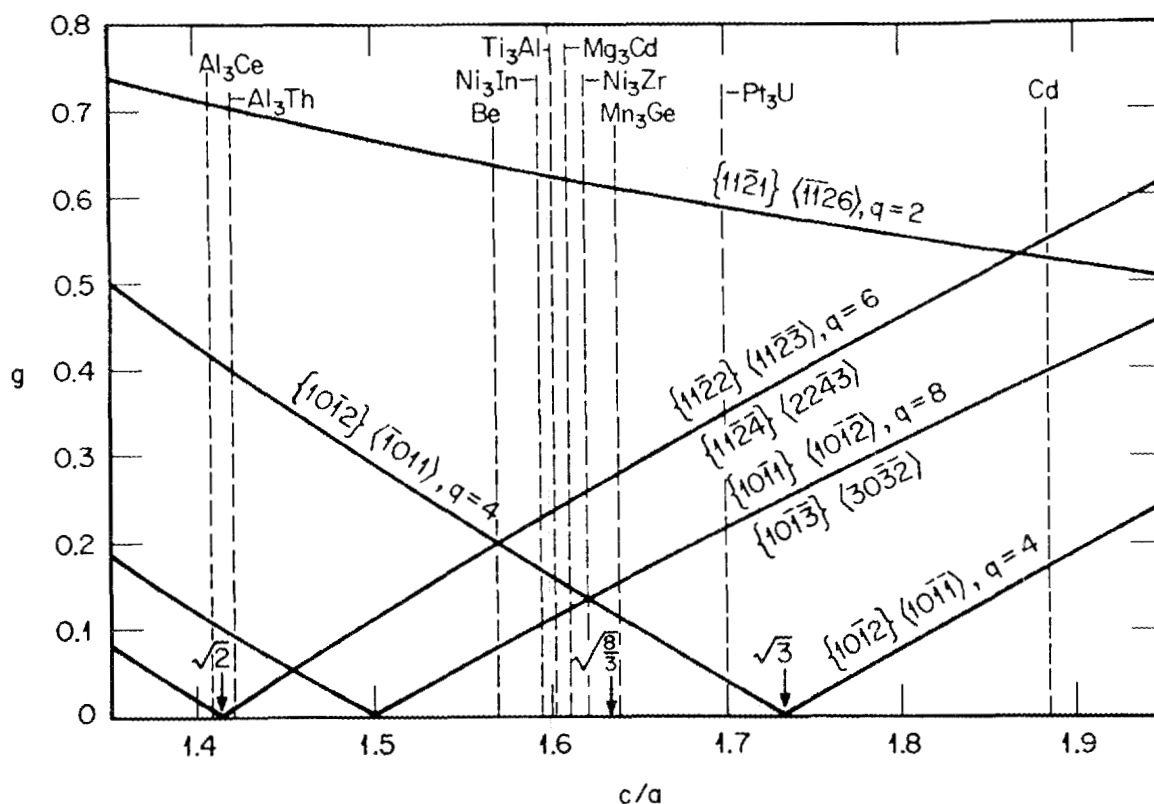


Fig. 13. Twinning shear of DO_{19} intermetallic compounds (A_3B).

viewpoint of the relative mobility of twinning dislocations, the primary twinning (fcc twinning) can be prevalent in $L1_0$ and DO_{22} alloys. This viewpoint is fully corroborated by the experimental findings in CuAu-I (ref. 52), TiAl (ref. 41), Ni_3V (ref. 53), and Al_3Ti (ref. 45).

The role of twinning in fracture of hcp metals discussed earlier⁵⁴ applies directly to the case of hexagonal DO_{19} alloys. When the necessary atom shuffling is considered by means of homogeneous shear of diatomic motifs, all the atoms must shuffle to a certain varying extent regardless of whether the crystal structure is chemically ordered or not. A coordinated motion of diatomic motifs of dissimilar atoms could actually be energetically more favorable than that of similar atoms.⁵¹ Therefore, the ease of twinning due to chemical ordering effects will vary from material to material. A number of DO_{19} compounds are shown on the $g - \lambda$ plot of Fig. 13, where $\lambda = c/a$, the axial ratio. The largest to

the smallest axial ratio corresponds to $\lambda = 1.70$ of Pt_3U and $\lambda = 1.41$ of Al_3Ce , respectively. There are many compounds which have $\lambda = 1.60$ to 1.63. In addition to those five shown in Fig. 13, there are Cd_3Mg , Co_3Mo , Fe_3Mn , Ni_3Sn , Ti_3Sn , Fe_3Ge , and Mn_3Sn . For a given compound, apart from the chemical effects, the lower the magnitude of g and/or q , the easier the twinning will become.

4. STRENGTHENING MECHANISMS

There are many physical sources of strengthening of ordered inter-metallic compounds.⁵⁵ In most of the alloys listed in Table 1, the peak temperature, T_p , of anomalous strengthening is closely related to the order-disorder transition temperature, T_c , such as in Cu_3Au , FeCo , Fe_3Al , $(\text{Ni,Fe,Co})_3\text{V}$, and Mg_3Cd .^{*} When deformation occurs primarily by twinning, e.g., in Fe_3Be , the flow stress tends to have a positive temperature dependence and a negative strain rate dependence.⁵⁷ As was discussed in Sect. 3.1, the source for the strengthening by pseudotwinning may be largely due to the restoring force of chemical origin. In this report, the focus of our discussion will be on the physical mechanisms for the anomalous temperature dependence of yield and flow stresses in $\text{Ni}_3\text{Al}^\dagger$ and $\beta\text{-CuZn}$ in which T_p is much lower than T_c (Table 3).

A schematic description of the yield stress, τ_y , as a function of deformation test temperature, T , at a certain strain rate, $\dot{\epsilon} > 10^{-4} \text{ s}^{-1}$, is given in Fig. 1. Table 3 lists the appropriate temperatures defined in Fig. 1 together with the melting point, T_m . The yield stress, τ_y , is referred to either the critical resolved shear stress (CRSS) of the primary slip system or the macroyield stress defined at the specific strain, usually $\epsilon = 0.002$.

^{*}Kornilov compounds (ref. 56).

[†]A Bertollide compound (ref. 56).

4.1 INTRINSIC EFFECTS

4.1.1 Anisotropy of APB Energy

The $\frac{1}{2}[\bar{1}01](010)$ APB energy in the $L1_2$ structure, γ_{010} , may be obtained from the difference between the ordering energies of an A_3B compound with the $L1_2$ and DO_{22} structures. Likewise, the $\frac{1}{2}[\bar{1}01](111)$ APB energy, γ_{111} , in the $L1_2$ structure is related to the phase stability with respect to the DO_{19} structure. The sign and magnitude of the APB energy is therefore a good measure of the phase stability.

In $L1_2$ alloys, the anisotropy of APB energies, $\gamma_{111}/\gamma_{010} > \sqrt{3}$, was defined as the necessary condition⁵⁸ for the cross-slip pinning model^{59,60} to explain the anomalous yield strength. Recently, there has been a number of APB energy evaluations for Ni_3Al . The data are summarized in Table 5.

The mechanical stability of an $\frac{1}{2}[101](111)$ type shear APB interface in the $L1_2$ structure can be analyzed in terms of the surface tension, per unit length along the z-axis (Fig. 14), defined by

$$T(\theta) = \gamma(\theta) + \frac{d^2\gamma}{d\theta^2}, \quad (5)$$

where θ is measured from the (010) plane. If we use the anisotropic γ function as before,³

$$\gamma(\theta) = \gamma_{010} + \frac{\sqrt{3}}{2} (\gamma_{111} - \gamma_{010}) \sin\theta, \quad (6)$$

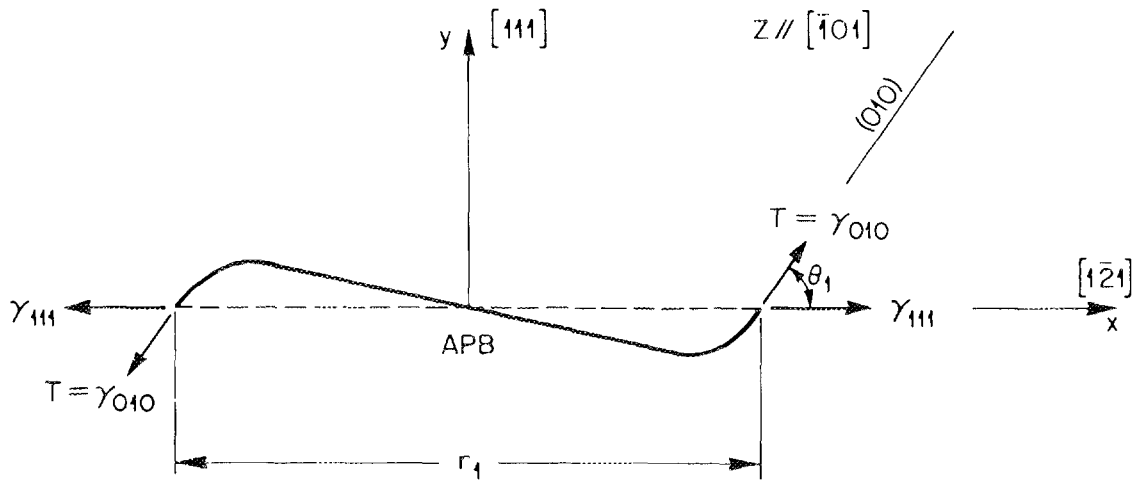
then the surface tension is a constant, $T = \gamma_{010}$. The deflection equation for a two-dimensional slab³ gives

$$y = ae^{\beta x} \sin \beta x, \text{ for } x > 0, \quad (7)$$

Table 5. APB Energy in Ni_3Al , γ_{hkl} (mJm^{-2})

γ_{111}	γ_{010}	$\gamma_{111}/\gamma_{010}$	Method	Ref.
111	90	1.2	Weak-beam TEM Atomistic simulation	23 61
142	83	1.7	Embedded atom method	62
96	28	3.4		63
280	197	1.4	Interchange potentials up to fourth near neighbors	64,65

ORNL-DWG 87-11926

Fig. 14. A stable equilibrium configuration of the (111) APB interface in the $L1_2$ structure.

$$\alpha = -\frac{r_1}{\pi} e^{-\pi} \frac{1}{\sqrt{6}}, \quad (8)$$

$$\beta = \frac{2\pi}{r_1}, \quad (9)$$

where r_1 is the periodicity of nonplanar APB interface. Figure 14 schematically depicts the stable equilibrium shape of an APB interface, which is based on the two continuous functions given by Eqs. (6) and (7). The γ anisotropy described by Eq. (6) is an approximation of first order.^{6,1} Nevertheless, this calculation and the one made earlier³ confirm the fact that the bending of an (111) APB interface in the L1₂ structure is necessary from the viewpoint of either the γ anisotropy or the interaction torque due to the elastic anisotropy.

Using the weak-beam TEM technique, Saka et al. (ref. 66) have recently determined the APB energy in β -CuZn to be $\gamma_{110} = 50 \text{ mJm}^{-2}$ and $\gamma_{112} = 37 \text{ mJm}^{-2}$ in the temperature range 77 K to 298 K. The anisotropy of $\gamma_{110}/\gamma_{112} = 1.4$ could be the driving force for the cross slip of $\frac{1}{2}\langle 111 \rangle$ screw superpartials from $\{1\bar{1}0\}$ planes to $\{11\bar{2}\}$ planes which Umakoshi et al. (ref. 67) have related to the yield strength anomaly in β -CuZn.

4.1.2 Interaction Torque

The interaction torque between two superpartial screw dislocations, $\underline{b} = \frac{1}{2}[\bar{1}01]$, in Ni₃Al has been identified as the principal driving force for the cross-slip pinning mechanism.¹⁹ The energetic criterion for the cross-slip pinning model was derived based on the combined anisotropy of elastic shear and APB energy^{9,19} as

$$\frac{3A}{A+2} \frac{\gamma_{111}}{\gamma_{010}} > \sqrt{3} \quad (10)$$

This is the necessary condition that should replace the earlier one, $\gamma_{111}/\gamma_{010} > \sqrt{3}$, proposed by Paidar et al. (ref. 58).

The elastic interaction energy between two parallel dislocations is obtained by evaluating the work done, V , in forming one dislocation at a location (r, θ) in the presence of the other at the origin. When this is done in an elastically anisotropic medium under the plane strain condition, one finds in general $V = V(r, \theta)$ (ref. 68). The radial and tangential components of the interaction force are obtained formally from $F_r = -\partial V / \partial r$ and $F_\theta = -(1/r) \partial V / \partial \theta$, respectively.

The physical source of the tangential component, F_θ , can be best understood by studying the displacement field of a screw dislocation. Figure 15 shows the sense and magnitude of the colinear vectorial difference between the anisotropic displacement field,²⁹ $\mu_z(\theta)$, and the isotropic field, $\mu_z^i(\theta) = b\theta/2\pi = (b/2\pi) \tan^{-1}(y/x)$, for the cases of the $L1_2$, B2, and DO_{19} structures. The positive and negative values of this difference, $\mu_z - \mu_z^i$, are related, respectively, to the forward ($+z$) and backward ($-z$) perturbation of u_z on the linear screw pitch of μ_z^i . No tangential force will result, $F_\theta = 0$, when an identical screw dislocation is situated on the certain planes of high symmetry, such that $\mu_z = \mu_z^i$. These planes are (010) and (101) of $L1_2$, $\{1\bar{1}0\}$ and $\{11\bar{2}\}$ of B2, and (0001) and ($\bar{1}100$) of the DO_{19} structure. In any plane which is oriented between the two planes mentioned above (Fig. 15), the tangential force arises because of the overlapping additional displacement of the same sign.

4.1.3 Dislocation Core Transformation

Although a dislocation core contributes only 5 to 10% of the total energy of a straight dislocation, the dislocation core configuration influences physical and mechanical properties strongly.⁶⁹ In the case of Ni_3Al , the configuration of a dissociated superdislocation depends on the energies of APB, SISF, superlattice extrinsic stacking fault (SESF), and complex stacking fault (CSF) on $\{111\}$ planes.⁷⁰ The SISF energy in Ni_3Al was determined experimentally²³ and by atomistic simulations⁶² to be $\gamma_{SISF} = 5 - 15 \text{ mJm}^{-2}$ and $\gamma_{SISF} = 13 \text{ mJm}^{-2}$, respectively. No evidence for CSF splitting by Shockley partials in Ni_3Al exists according to

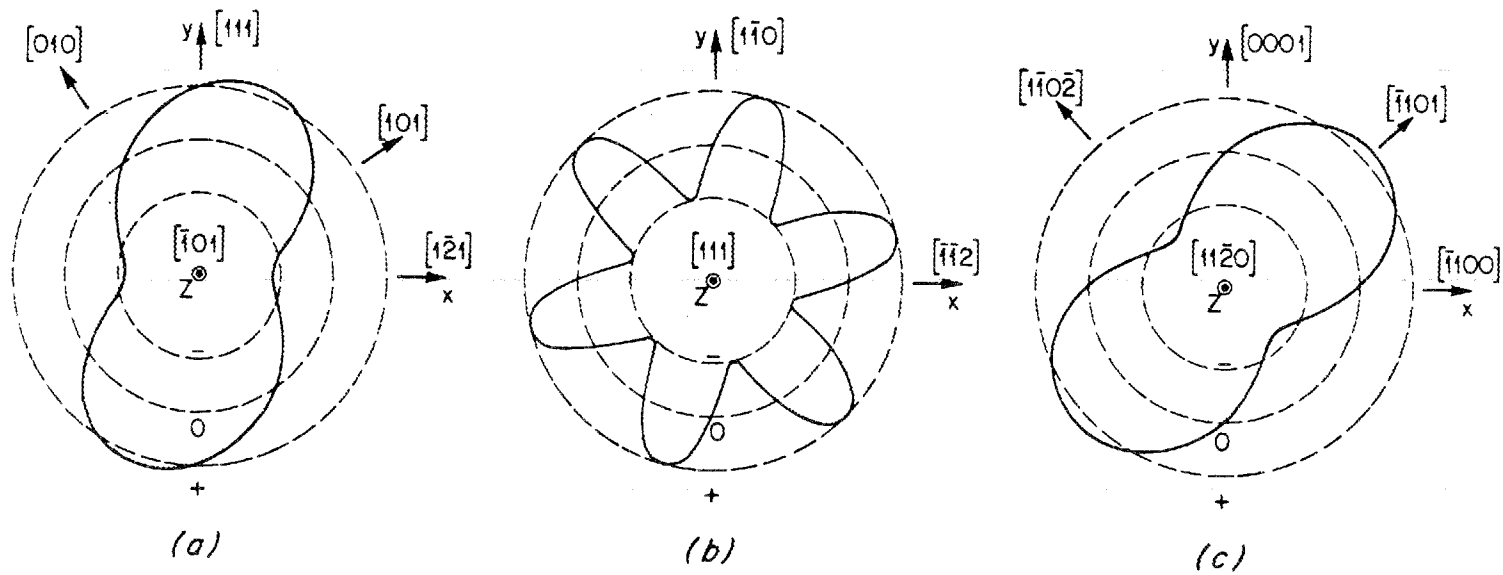


Fig. 15. Anisotropic displacement $\mu_z^i - \mu_z$ of a screw dislocation; (a) $\underline{b} = \frac{1}{2}[\bar{1}01]$ in $L1_2$, (b) $\underline{b} = \frac{1}{2}[111]$ in $B2$, and (c) $\underline{b} = \frac{1}{3}[11\bar{2}0]$ in the DO_{19} structure.

the direct observation by TEM^{5,23} and atom probe field ion microscopy (APFIM).^{71,72} Therefore, the twofold dissociation of superdislocations discussed in Sect. 2.1 is consistent with the experimental observations. In the computer simulation analysis of dissociation and core structure of screw superdislocations in A₃B (Ni₃Al-like) alloys,^{26,27} the two ratios of the CSF energy to the APB energy on {111} planes used for the A-B potentials were 1.3 and 1.9.

In the case of bcc-based ordered alloys, no stable stacking faults other than APBs exist, and therefore the dissociation analysis made in Sect. 2.2 is also a realistic description.

4.1.4 Yield Stress

4.1.4.1 Ni₃Al

The schematic diagram of Fig. 1 for τ_y vs T applies generally for single crystals and polycrystals of Ni₃Al. The maximum stress at T_p was $\tau_p \approx 360$ MPa for both the CRSS of {111}< $\bar{1}01$ > slip in a single crystal at the neutral orientation⁷³ (tension = compression) and the compressive yield stress (0.2% offset) in a polycrystalline alloy⁷² of grain size $d = 85$ μm . Weihs et al. (ref. 74) found that grain refinement further strengthens the alloy at low temperatures and weakens it at high temperatures. Miura et al. (ref. 75) found no strain rate sensitivity for $d = 275$ μm , but a sensitive strain rate dependence for $d = 4$ μm . In the fine-grain alloy under the slower strain rate ($\dot{\epsilon} = 1.4 \times 10^{-5}$ s⁻¹), an apparent stress relaxation at high temperatures was attributed to grain boundary sliding.⁷⁵

Effects of strain rate on τ_y vs T in Ni₃Al single crystals were found as follows: (a) virtually no change in τ_y , the CRSS of {111}< $\bar{1}01$ > slip, at low temperatures (the region II of Fig. 1) was noted,⁷⁵⁻⁷⁸ and (b) a large increase in τ_y , the CRSS of {010}< $\bar{1}01$ > slip, at high temperatures (the region III of Fig. 15) with increasing $\dot{\epsilon}$ was observed.⁷⁵⁻⁷⁸ In the temperature region II of Fig. 1, therefore, τ_y is related to the force opposing the dislocation motion, which is the intrinsic property of

superlattice dislocations, but not to the dislocation microstructure which depends on the applied strain rate. Accordingly, τ_b , may be related to the mechanical threshold, the "plane glide resistance" of the material,⁷⁹ and $\partial\tau_y/\partial T$ at $T > T_b$ may be associated with the increase in the plane glide resistance with increasing temperature.

The main concept of the force couplet model, which is introduced to account for the positive temperature dependence of $\partial\tau_y/\partial T$ (refs. 3,9,80), can be outlined as follows:

1. The "line glide resistance" (ref. 79) of a superdislocation arises from a product of the edge stress, τ_{xy} in Fig. 3, and the cross-sectional area displaced by the bending of an APB interface, A_d of Eq. (15) in ref. 3.
2. The effective APB energy is obtained by subtracting from the nonequilibrium APB energy during the slip process, γ_{111} , the difference in total force on the two superpartials,

$$\begin{aligned}\gamma_{111}^e &= \gamma_{111} - [\tau_{zy}b - \text{sgn}(\tau_{xy}) \cdot F_\ell]_2 + [\tau_{zy}b - F_\ell]_1, \quad (11) \\ &= \gamma_{111} + F_\ell[\text{sgn}(\tau_{xy}) - 1],\end{aligned}$$

where $F_\ell = \tau_{xy}A_d/2b$.

3. The increasing number of cross-slipped pinning segments with increasing temperature can result in drag of both the leading and the trailing superpartials. In the expression of the driving force for cross-slip pinning, Eq. (2) of ref. 19, γ_{111} should be replaced by γ_{111}^e of Eq. (11).
4. The plane glide resistance due to the cross-slip pinning, $\tau_{p\ell}$, can be obtained from Eqs. (4-6) of ref. 19.

4.1.4.2 β -CuZn

The model introduced by Brown,⁸¹ and modified by others,⁸²⁻⁸⁵ that the temperature dependence of τ_y in the B2 alloys is directly related to the change in the local LRO across the APB interface, is simply the "element glide resistance" (ref. 79)

$$\tau_{e\ell} = \tau_0 + \Delta\gamma_{hkl}^e / 2b \quad , \quad (12)$$

where τ_0 is the lattice resistance to the individual superpartials, and $\Delta\gamma_{hkl}^e$ is the difference between the APB energy of the (hkl) plane created by the leading superpartial and that eliminated by the trailing superpartial. The total glide resistance, the CRSS or the yield stress, in the region II is obtained by a superposition of the two types of linear barriers,

$$\tau_y^{II} = \langle \tau_{e\ell} \rangle + \langle \tau_{p\ell} \rangle \quad , \quad (13)$$

where the bracket denotes the average over the primary slip system. The force couplet model outlined above is a general model for any case of twofold dissociation of a superdislocation including the two cases of Fig. 8 for the B2 structure. Since no nonglide stress exists on $\{1\bar{1}0\}$ planes, and hence $\gamma_{110} = \gamma_{110}$, $\tau_{p\ell}$ arises only if $\gamma_{110} > \gamma_{112}$. In the $\{11\bar{2}\}\langle 111 \rangle$ slip system, on the other hand, the interaction torque promotes self-climb of the two superpartials away from each other as in Fig. 10(e). The thermally activated formation of double jogs on the edge superpartials and its contribution to the yield strength anomaly can be formulated within the framework of the force couplet model.⁸⁰

The yield stress in the temperature region II (Fig. 1) predicted by the force couplet model is schematically summarized in Fig. 16. Here, the yield stress is normalized to the shear modulus, μ , which is taken to be

ORNL-DWG 87-11924

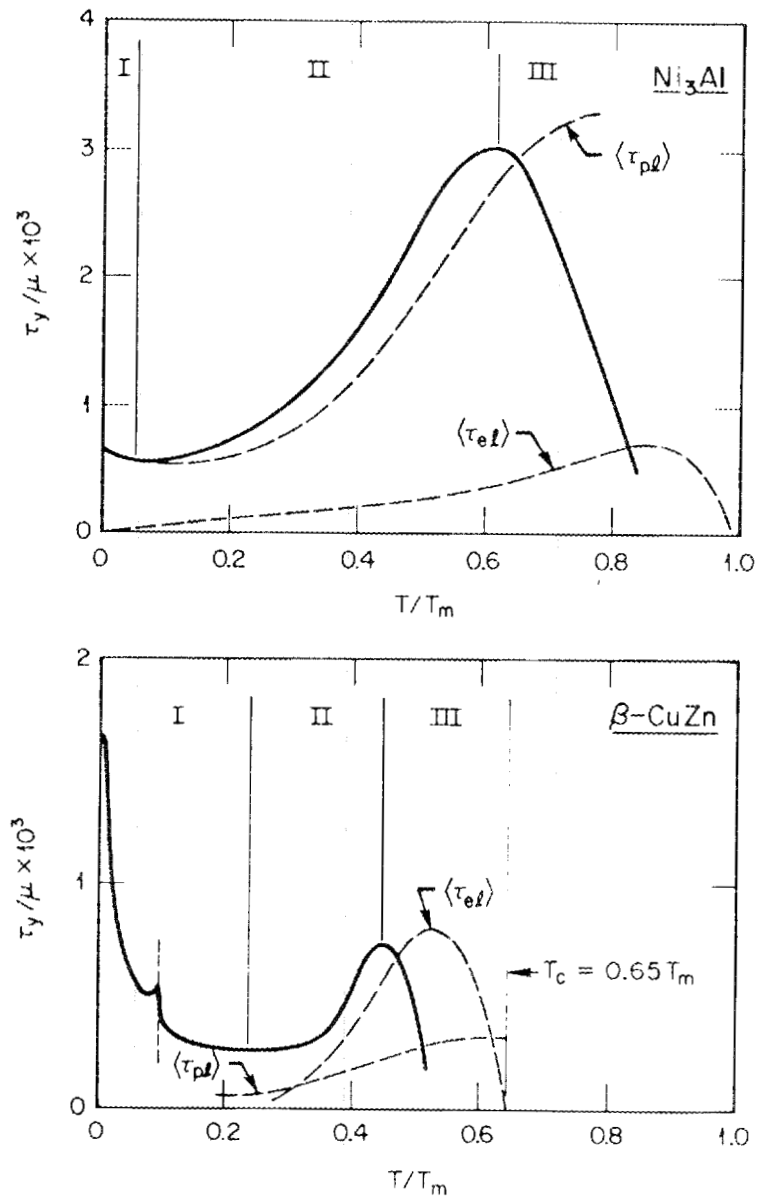


Fig. 16. Contribution of τ_y^{II} obtained by the force couplet model to the yield strength, τ_y , (a) Ni_3Al and (b) $\beta\text{-CuZn}$.

the room temperature value of C_{44} (Table 2). Whereas the cross-slip pinning mechanism, $\langle \tau_{pl} \rangle$, dominates τ_y in Ni_3Al , the fault dragging mechanism, $\langle \tau_{el} \rangle$, dominates τ_y in $\beta-CuZn$. A slight decrease in $\partial \langle \tau_{pl} \rangle / \partial T$ at high temperatures is due to the temperature dependence of the elastic constants.^{13,19}

In the region I of $\beta-CuZn$, temperature and strain rate dependences of τ_y are essentially the same as in bcc metals.^{86,87} The discontinuity of $\partial \tau_y / \partial T$ around 170 K is associated with the transition from the twin $\{112\}$ slip to the $\{110\}$ slip, where the former gives rise to a slightly positive temperature dependence.

At higher temperatures, in region III, the active slip systems are $\{010\} \langle \bar{1}01 \rangle$ for Ni_3Al and $\{110\} \langle 001 \rangle$ for $\beta-CuZn$. No driving force for the cross-slip mechanism exists, in these cases, because neither the reduction in APB energy, nor the interaction torque is involved. Therefore, the negative temperature dependence must be related to the fault dragging mechanisms, $\langle \tau_{el} \rangle$, associated with these respective slip systems. In the region III, i.e., $T > 0.6 T_m$ for Ni_3Al , the formation and migration of vacancies are sufficiently high to cause the climb dissociation of superdislocation pairs.^{28,31} The resulting viscous glide mechanism is then responsible for the positive strain rate sensitivity.⁵¹

4.2 EFFECTS OF NONSTOICHIOMETRY AND ALLOYING

Compositional deviations from stoichiometry often lead to strengthening at low temperatures^{40,88-92} viz., defect hardening. It is assumed that the elastic constants do not change significantly with the varying degree of nonstoichiometry. This assumption is justified for the Ni_3Al system because of the moderate differences in the elastic constants between Ni_3Al and $NiAl$ (Table 2). Therefore, according to the force couplet model, the source of defect hardening in the region II must be from the change in γ'_{111} by relaxation of the degree of LRO, or by segregation of one type of the constituent atoms. As γ'_{111} and γ^e_{111} are

lowered, Eq. (11), $\tau_{e\ell}$ increases and $\tau_{p\ell}$ decreases according to Eq. (12) and Eqs. (4-6) of ref. 19, respectively, such that a variety of nonstoichiometry effects on τ_y vs T will result as were observed in Ni_3Al , Ni_3Ga , Ni_3Si , and Ni_3Ge (refs. 91,92).

Since defect hardening was found to be much more for aluminum-rich deviations than for nickel-rich deviations,⁸⁸⁻⁹² Mishima et al. (ref. 93) made a systematic investigation of ternary additions of the transition elements that are expected to substitute aluminum sites in Ni_3Al (ref. 94). All the transition elements added to Ni_3Al showed strengthening, viz., solution hardening. The rate of solution hardening, $\partial\tau_y/\partial c$ in units of MPa/at. %, was determined at 77 K to be the lowest, 20 for titanium and 140, the highest, for hafnium.⁹³ Such a marked difference resulting from a pair of chemically similar solute species cannot be fully resolved by the current theory of solution hardening.

Let us recall Fig. 4(d) and Fig. 11(b) to discuss the formation of microtwins and the solute effects on the configuration of dislocation dissociation. In a situation under the edge stress of $\tau_{xy} < 0$ as in Fig. 4(d), nucleation of SISF loop near the trailing superpartial is possible, which consists of four layers of the Ni_3Sn type (DO_{19}) structure. This loop can activate the reflection mechanism to form a three-layer microtwin.⁹⁵ Coplanar microtwins of this kind can combine, with the aid of cross slip, as in Fig. 4(e), to develop macrotwins. The twin formation observed in γ' - Ni_3Al precipitate particles in nickel-base superalloys^{96,97} is consistent with the mechanism described above. In an analogous manner, the formation of a SESF loop is also possible, which consists of seven layers of the Ni_3Ti (DO_{24}) type structure.⁹⁷

In view of the force couplet model, then, the strengthening effects by both nonstoichiometry and ternary alloying additions arise from the segregation of the minority and/or substitutional atoms to the APB and their tendency to nucleate a faulted sessile loop near the trailing superpartial. This combined effect may be the reason for the apparent

synergistic strengthening of the ternary additions and aluminum-rich nonstoichiometry reported by Rawlings and Staton-Bevan.^{8,9} The growth of those sessile loops and concomitant local disordering will lead to a distribution of loops in the midst of unpaired dislocations. This is what has been observed (Fig. 17) during the recent in situ deformation TEM experiment.⁵

Finally, in addition to substitutional solute strengthening, a high strengthening by boron addition was found in Ni₃Al prepared by rapid solidification.^{9,8} Boron can be dissolved into Ni₃Al up to about 1.5 at. %, and tends to occupy the octahedral interstitial site.^{9,9} The recent APFIM investigation^{7,2} showed that boron segregates to dislocations and APB interfaces. Therefore, drag of a Cottrell atmosphere and/or Suzuki locking are possible mechanisms for the potent strengthening by boron additions at ambient temperatures.

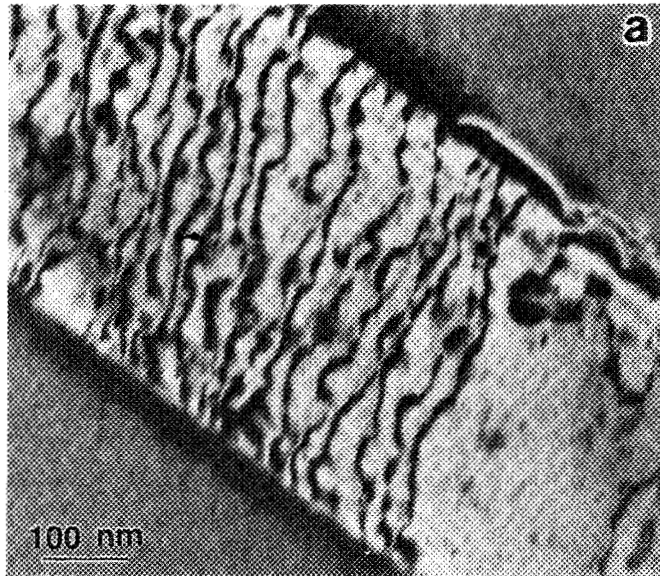
5. DISCUSSION

5.1 ANOMALOUS YIELD STRENGTH

In Ni₃Al, Thornton et al. (ref. 100) measured the temperature dependence of microyield stress over a strain range, $\epsilon = 10^{-6} - 10^{-2}$, and found that only τ_y at $\epsilon \geq 10^{-4}$ was strongly temperature dependent. This observation was interpreted by Kear and Oblak^{7,0} on the basis of the disparity of mobility between the edge and screw segments. Since the disparity is further widened by the presence of interaction torque, the force couplet model reinforces the basis for the above interpretation. This interpretation is valid for those systems in which the cross-slip pinning mechanism, τ_{pl} , dominates the contribution to τ_y .

On the other hand, in β -CuZn which is considered to have τ_y due mainly to the APB and/or microtwin dragging mechanism, τ_{el} , the force couplet model predicts the same temperature dependence of τ_y for

VP6059



YP6057

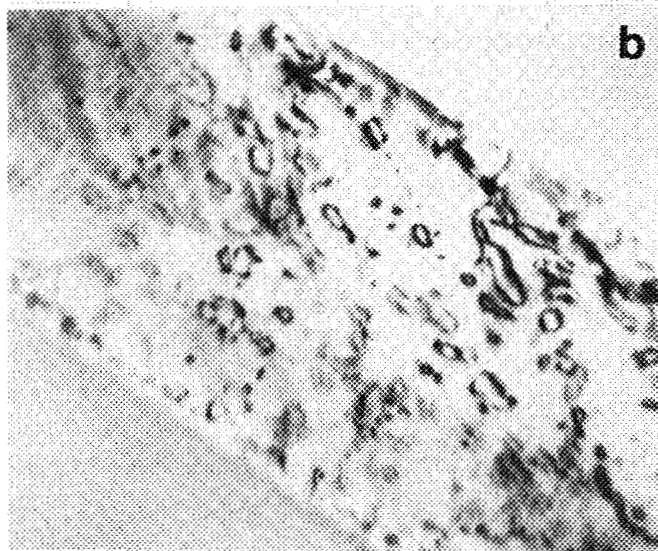


Fig. 17. A disordered region of the slip band observed in Ni_3Al under load showing (a) unpaired glide dislocations and (b) sessile loops under two different diffracting conditions.

micro- and macro-yielding, i.e., regardless of the magnitude of microstrain. This has been confirmed recently by Ito and Nakayama¹⁰¹ who used the etch pit technique to characterize the microyield strength of β -CuZn.

Both the orientation dependence^{102,103} and the tension/compression asymmetry^{103,104} of τ_y vs T relationships in the L1₂ type alloys were treated in the model proposed by Paidar et al. (ref. 58). In addition, according to the force couplet model, both the element and the plane glide resistances, τ_{el} and τ_{pl} , are sensitively dependent on the sign and the magnitude of nonglide stress, τ_{xy} , via the effective fault energy, Eq. (11). This new effect will be elaborated further in a detailed analysis.⁸⁰

5.2 STRAIN RATE EFFECT

The yield strength, τ_y , in the region II of Ni₃Al is expected to be virtually insensitive to the applied strain rate because the number density of pinning centers, or cross-slipping segments, along screw dislocations is independent of the dislocation velocity. On the other hand, the element glide resistance, τ_{el} , due to the shear fault (APB, SISF, or microtwin) dragging mechanism is expected to show a negative strain rate dependence as in the case of deformation by twinning. No study has been made on the strain rate sensitivity of τ_y in the region II of a material in which τ_{el} is more important than τ_{pl} , e.g., β -CuZn.

5.3 ORDER TWINNING

The full implication of the conjugate relationship between the active slip mode at high temperatures (the region III) and the order twinning has yet to emerge. In the region III of Ni₃Al, where the $\{010\}\langle\bar{1}01\rangle$ slip system is active, the normal negative temperature dependence and positive strain rate sensitivity of τ_y are observed. This indicates that the energetic and kinetic mechanisms for the order twinning may be clearly different from those for the primary twinning. It is conceivable that

high temperature mechanical properties can be improved through a better understanding of this slip-twinning conjugate relationship, particularly in the bcc-based and noncubic intermetallic systems.

5.4 ALLOY HARDENING

As was mentioned in Sect. 4.2, in order to fully ascertain the physical mechanism of solution hardening, some pertinent defect properties are required, e.g., in Ni_3Al , the occupation sites of hafnium and titanium atoms and the spatial distribution of boron atoms. Whereas an ion channeling and Rutherford backscattering study⁹⁹ indicated that the majority of hafnium atoms are on the nickel sublattice, the recent investigations by APFIM¹⁰⁵ and the electron channeling technique¹⁰⁶ showed that hafnium has a strong preference for the aluminum sites.

5.5 DISLOCATION MOBILITY

We have emphasized the experimental results of dislocation configurations under stress obtained from in situ deformation TEM investigations. In addition, the use of complementary techniques to study dislocation mobility, e.g., etch pit and X-ray topography techniques, would be meaningful. A dislocation dissociation analysis can begin with the geometry expected from the hard sphere model, taking account of the relative size differences amongst the constituent atoms. Only atomistic simulation studies of the dislocation core structures will reveal the full details of the physical sources of dislocation mobility. However, in such a study, extreme care must be exercised in setting the boundary conditions to be in compliance with the displacement field (Fig. 15) given by anisotropic elasticity theory.

6. SUMMARY

The newly developed force couplet model for the anomalous strengthening at intermediate temperatures (the region II) is summarized as follows:

1. The yield strength arises from two sources of the glide resistance, the fault dragging mechanism (the element glide resistance), τ_{el} , and the cross-slip pinning mechanism (the plane glide resistance), τ_{pl} .
2. The effective fault energy, γ^e , consists of two terms related to the chemical and mechanical instability of a shear fault.
3. As γ^e is lowered by solute segregation and/or high nonglide stress, τ_{el} increases and τ_{pl} decreases.
4. The major aspects of anomalous temperature dependence, strain rate effect, in situ deformation TEM observations, and nonstoichiometry effect are all accounted for by the present model.

In addition, the conjugate relationship between the order twinning and the secondary slip systems is identified in all the ordered structures considered. This relationship will play an important role in the deformation by viscous glide at high temperatures (the region III).

ACKNOWLEDGMENTS

The authors would like to thank J. Bentley, P. Veyssi re, F. E. Heredia, and D. P. Pope for helpful discussions; Connie Dowker for typing the draft; and Glenda Carter for manuscript preparation.

REFERENCES

1. C. C. Koch, C. T. Liu, and N. S. Stoloff, eds., *High-Temperature Ordered Intermetallic Alloys Materials, Research Society Symposia Proceedings*, Vol. 39, Materials Research Society, Pittsburgh, Pa., 1985.
2. N. S. Stoloff, C. C. Koch, C. T. Liu, and O. Izumi, eds., *High-Temperature Ordered Intermetallic Alloys, Materials Research Society Symposia Proceedings*, Vol. 81, Materials Research Society, Pittsburgh, Pa., 1987.
3. M. H. Yoo, *Acta Metall.* **35**, 1559 (1987).
4. I. Baker, J. A. Horton, and E. M. Schulson, *Philos. Mag. Lett.* **55**, 3 (1987).
5. J. A. Horton, M. H. Yoo, and I. Baker, *Philos. Mag.* (to be submitted).
6. A. Nohara, T. Imura, and H. Saka, *Scr. Metall.* **18**, 1267 (1984).
7. A. Nohara and T. Imura, *Phys. Status Solidi A* **91**, 559 (1985).
8. T. Imura, pp. 381-97 in *In Situ Experiments with High Voltage Electron Microscopes*, ed. H. Fujita, Osaka University, Osaka, Japan, 1985.
9. M. H. Yoo, "Effects of Elastic Anisotropy in the Anomalous Yield Behavior of Cubic Ordered Alloys," p. 207 in *High-Temperature Ordered Intermetallic Alloys, Materials Research Society Symposia Proceedings*, Vol. 81, eds. N. S. Stoloff, C. C. Koch, C. T. Liu, and O. Izumi, Materials Research Society, Pittsburgh, Pa., 1987.
10. D. P. Pope and S. S. Ezz, *Int. Metall. Rev.* **29**, 136 (1984).
11. M. Yamaguchi and Y. Umakoshi, *The Structure and Properties of Crystal Defects*, eds. V. Paidar and L. Lejcek, Elsevier Science Publishing, New York, 1984, p. 131.
12. C. T. Liu, *Int. Metall. Rev.* **29**, 168 (1984).
13. M. Yamaguchi and Y. Umakoshi, *Intermetallic Compounds*, Daily Industrial Press (in Japanese), 1984.
14. D. M. Wee, O. Noguchi, Y. Oya, and T. Suzuki, *Trans. Japan Inst. Met.* **21**, 237 (1980).

15. References of elastic constants:
- (a) F. X. Kayser and C. Stassis, *Phys. Status Solidi A* **64**, 335 (1981);
 - (b) P. Turchi, F. Plicque, and Y. Calvayrac, *Scr. Metall.* **9**, 797 (1975);
 - (c) P. A. Flinn, G. M. McManus, and J. A. Rayne, *J. Phys. Chem. Solids* **15**, 189 (1960);
 - (d) H. J. Leamy, E. D. Gibson, and F. X. Kayser, *Acta Metall.* **15**, 1827 (1967);
 - (e) R. J. Wasilewski, *Trans. Am. Inst. Min., Metall., Pet. Eng.* **236**, 455 (1966);
 - (f) Y. A. Chang, L. Himmel, and J. P. Neumann, *J. Appl. Phys.* **38**, 649 (1967);
 - (g) G. M. McManus, *Phys. Rev.* **129**, 2004 (1963);
 - (h) H. B. Huntington, *Solid State Phys.*, eds. F. Seitz and D. Turnbull, Vol. 7, Academic Press, New York, 1958, p. 276;
 - (i) F. B. Bateman, H. J. McSkimin, and J. M. Whelan, *J. Appl. Phys.* **30**, 544 (1959);
 - (j) S. Zirinski, *Acta Metall.* **4**, 164 (1956);
 - (k) J. B. Rausch and F. X. Kayser, *J. Appl. Phys.* **48**, 487 (1977);
 - (l) C. H. Cheng, *J. Phys. Chem. Solids* **28**, 413 (1967);
 - (m) F. Wallow, G. Neite, W. Schröder, and E. Nembach, *Phys. Status Solidi A* **99**, 483 (1987).
16. J. P. Hirth and J. Lothe, *Theory of Dislocations*, Wiley-Interscience, New York, 1982, pp. 221, 650, 688.
- 17. A. Ball and R. E. Smallman, *Acta Metall.* **14**, 1517 (1966).
 - 18. D. I. Porter, *J. Mater. Sci.* **5**, 201 (1969).
 - 19. M. H. Yoo, *Scr. Metall.* **20**, 915 (1986).
 - 20. N. S. Stoloff and R. G. Davies, *Prog. Mater. Sci.* **13**, 3 (1966).
 - 21. M. S. Duesbery, *Acta Metall.* **31**, 429 (1983).
 - 22. M. S. Duesbery, *Proc. R. Soc. London. Ser. A* **392**, 145 (1984).
 - 23. J. Douin, P. Veyssiére, and P. Beauchamp, *Philos. Mag. A* **54**, 375 (1986).
 - 24. P. A. Flinn, *Trans. The Metall. Soc., Am. Inst. Min., Metall., Pet. Eng.* **218**, 145 (1960).
 - 25. J. A. Horton and C. T. Liu, *Acta Metall.* **33**, 2191 (1985).

26. M. Yamaguchi, V. Paidar, D. P. Pope, and V. Vitek, *Philos. Mag. A* **45**, 867 (1982).
27. V. Paidar, M. Yamaguchi, D. P. Pope, and V. Vitek, *Philos. Mag. A* **45**, 883 (1982).
28. P. Veyssi re, *Philos. Mag. A* **50**, 189 (1984).
29. V. Vitek, *Crystal Lattice Defects* **5**, 1 (1974).
30. M. H. Yoo and B.T.M. Loh, *J. Appl. Phys.* **43**, 1373 (1972).
31. H. Saka and Y. M. Zhu, *Philos. Mag. A* **51**, 629 (1985).
32. H. L. Fraser, R. E. Smallman, and M. H. Loretto, *Philos. Mag.* **28**, 651 (1973).
33. M. G. Mendiratta, H. M. Kim, and H. A. Lipsitt, *Metall. Trans.* **15A**, 395 (1984).
34. H. Saka and M. Kawase, *Philos. Mag.* **49**, 525 (1984).
35. H. Saka, Y. M. Zhu, M. Kawase, A. Nohara, and T. Imura, *Philos. Mag.* **51**, 365 (1985).
36. A. K. Head, *Phys. Status Solidi* **19**, 185 (1967).
37. Y. T. Chou and G. T. Sha, *Metall. Trans.* **3**, 2857 (1972).
38. R. C. Crawford, T.L.F. Ray, and D. J. H. Cockayne, *Philos. Mag.* **27**, 1 (1973).
39. P. R. Strutt, R. S. Polvani, and J. C. Ingram, *Metall. Trans.* **7A**, 23 (1976).
40. Y. Umakoshi, M. Yamaguchi, and T. Yamane, *Philos. Mag.* **52**, 357 (1985).
41. H. A. Lipsitt, D. Shechtman, and R. E. Schafrik, *Metall. Trans.* **6A**, 1991 (1975).
42. A. Faress and G. Vanderschaeve, *Acta Metall.* **35**, 691 (1987).
43. M. Yamaguchi, Y. Umakoshi, and T. Yamane, "Deformation of the Intermetallic Compound Al_3Ti and Some Alloys with an Al_3Ti Base," p. 275 in *High-Temperature Ordered Intermetallic Alloys, Materials Research Society Symposia Proceedings*, Vol. 81, eds. N. S. Stoloff, C. C. Koch, C. T. Liu, and O. Izumi, Materials Research Society, Pittsburgh, Pa., 1987.
44. T. Kawabata, T. Kanai, and O. Izumi, *Acta Metall.* **33**, 1355 (1985).
45. M. Yamaguchi, Y. Umakoshi, and T. Yamane, *Philos. Mag. A* **55**, 301 (1987).

46. M. H. Yoo and B. T. M. Loh, *Numerical Calculations of Elastic Properties for Straight Dislocations in Anisotropic Crystals*, ORNL/TM-3408, Oak Ridge National Laboratory, July 1971.
47. M. H. Yoo and B. T. M. Loh, *Fundamental Aspects of Dislocation Theory*, eds. J. A. Simmons, R. deWit, and R. Bullough, US-NBS Spec. Publ. 317, Vol. I, 1970, p. 479.
48. V. S. Arunachalam and C. M. Sargent, *Scr. Metall.* **5**, 949 (1971).
49. S. Mahajan and D. F. Williams, *Int. Metall. Rev.* **18**, 43 (1973).
50. S. B. Chakraborty and E. A. Starke, Jr., *Acta Metall.* **23**, 63 (1975).
51. M. H. Yoo, unpublished data.
52. D. W. Pashley, J. L. Robertson, and M. J. Stowell, *Philos. Mag.* **19**, 83 (1969).
53. G. Vanderschaeve and B. Escaig, *Philos. Mag. A* **48**, 265 (1983).
54. M. H. Yoo, *Metall. Trans.* **12A**, 409 (1981).
55. N. S. Stoloff, *Strengthening Methods in Crystals*, eds. A. Kelly and R. B. Nicholson, Appl. Sci. Publ., London, 1971, p. 193.
56. L. L. Kornilov, *Intermetallic Compounds*, ed. J. H. Westbrook, John Wiley & Sons Inc., New York, 1967, p. 349.
57. R. E. Reed-Hill, *The Inhomogeneity of Plastic Deformation*, American Society for Metals, Metals Park, Ohio, 1971, p. 285.
58. V. Paidar, D. P. Pope, and V. Vitek, *Acta Metall.* **32**, 435 (1984).
59. B. H. Kear and H. G. F. Wilsdorf, *Trans. The Metall. Soc., Am. Inst. Min., Metall. Pet. Eng.* **224**, 382 (1962).
60. S. Takeuchi and E. Kuramoto, *Acta Metall.* **21**, 415 (1973).
61. P. Beauchamp, J. Douin, and P. Veyssi re, *Philos. Mag.* **55**, 565 (1987).
62. S. P. Chen, A. F. Voter, and D. J. Srolovitz, *Scr. Metall.* **20**, 1389 (1986).
63. S. M. Foiles and M. S. Daw, *J. Mater. Res.* **2**, 5 (1987).
64. G. Inden, S. Bruns, and H. Ackermann, *Philos. Mag.* **53**, 87 (1986).
65. G. M. Stocks and M. H. Yoo, unpublished data.

66. H. Saka, M. Kawase, A. Nohara, and T. Imura, *Philos. Mag. A* **50**, 65 (1984).

67. Y. Umakoshi, M. Yamaguchi, Y. Namba, and K. Murakami, *Acta Metall.* **24**, 89 (1976).

68. A. N. Stroh, *Philos. Mag.* **3**, 625 (1958).

69. V. Vitek, *Dislocations and Properties of Real Materials*, The Institute of Metals, London, 1985, p. 30.

70. B. H. Kear and J. M. Oblak, *J. de Physique C7*, **35** (1974).

71. R. J. Taunt and B. Ralph, *Philos. Mag.* **30**, 1379 (1974).

72. J. A. Horton and M. K. Miller, "An Atom Probe Study of Boron Segregation to Line and Planar Defects in Ni₃Al," p. 105 in *High-Temperature Ordered Intermetallic Alloys, Materials Research Society Symposia Proceedings*, Vol. 81, eds. N. S. Stoloff, C. C. Koch, C. T. Liu, and O. Izumi, Materials Research Society, Pittsburgh, Pa., 1987.

73. F. E. Heredia and D. P. Pope, "Strengthening of Ni₃Al by Ternary Additions," p. 213 in *High-Temperature Ordered Intermetallic Alloys, Materials Research Society Symposia Proceedings*, Vol. 81, eds. N. S. Stoloff, C. C. Koch, C. T. Liu, and O. Izumi, Materials Research Society, Pittsburgh, Pa., 1987.

74. T. P. Weihs, V. Zinoviev, D. V. Viens, and E. M. Schulson, *Acta Metall.* **35**, 1109 (1987).

75. T. Suzuki, Tokyo Institute of Technology, Yokohama, Japan, private communication to M. H. Yoo, Oak Ridge National Laboratory, Oak Ridge, Tenn., December 3, 1986.

76. G. R. Leverant, M. Gell, and S. W. Hopkins, *J. Mater. Sci.* **8**, 125 (1971).

77. Y. Umakoshi, D. P. Pope, and V. Vitek, *Acta Metall.* **32**, 449 (1984).

78. J. K. Tien, S. Eng, and J. M. Sanchez, "An Overview of the Temperature Dependence of the Strength of the Ni₃Al System," p. 183 in *High-Temperature Ordered Intermetallic Alloys, Materials Research Society Symposia Proceedings*, Vol. 81, eds. N. S. Stoloff, C. C. Koch, C. T. Liu, and O. Izumi, Materials Research Society, Pittsburgh, Pa., 1987.

79. U. F. Kocks, A. S. Argon, and M. F. Ashby, *Thermodynamics and Kinetics of Slip*, Pergamon Press, Oxford, 1975.

80. M. H. Yoo, unpublished data.
81. N. Brown, *Philos. Mag.* **4**, 693 (1959).
82. M. J. Marcinkowski and R. M. Fisher, *J. Appl. Phys.* **34**, 2135 (1963).
83. L. E. Popov, E. V. Kozlov, and N. S. Golosov, *Phys. Status Solidi* **13**, 569 (1966).
84. A. Nohara and T. Imura, *Japan J. Appl. Phys.* **25**, 25 (1986).
85. J. M. Sanchez, S. Eng, Y. P. Wu, and J. K. Tien, "Modeling of Antiphase Boundaries in $L1_2$ Structures," p. 57 in *High-Temperature Ordered Intermetallic Alloys, Materials Research Society Symposia Proceedings*, Vol. 81, eds. N. S. Stoloff, C. C. Koch, C. T. Liu, and O. Izumi, Materials Research Society, Pittsburgh, Pa., 1987.
86. S. Hanada and O. Izumi, *Phys. Status Solidi A* **40**, 589 (1977).
87. S. Takeuchi, T. Hashimoto, K. Suzuki, and M. Ishihara, *Acta Metall.* **30**, 513 (1982).
88. R. W. Guard and J. H. Westbrook, *Trans. Am. Inst. Min., Metall., Pet. Eng.* **215**, 807 (1959).
89. R. D. Rawlings and A. E. Staton-Bevan, *J. Mater. Sci.* **10**, 505 (1975).
90. K. Aoki and O. Izumi, *Phys. Status Solidi A* **38**, 587 (1976).
91. O. Noguchi, Y. Oya, and T. Suzuki, *Metall. Trans.* **12A**, 1647 (1981).
92. T. Suzuki, Y. Oya, and S. Ochiai, *Metall. Trans.* **15A**, 173 (1984).
93. Y. Mishima, S. Ochiai, M. Yodogawa, and T. Suzuki, *Trans. Japan Inst. Met.* **27**, 41 (1986).
94. S. Ochiai, Y. Oya, and T. Suzuki, *Acta Metall.* **32**, 289 (1984).
95. S. Mahajan and G. Y. Chin, *Acta Metall.* **21**, 1353 (1973).
96. A. Guimier and J. L. Strudel, *Proc. of Second Int. Conf. on The Strength of Metals and Alloys*, Asilomar, Vol. 3, American Society for Metals, Metals Park, Ohio, 1970, p. 1145.
97. B. H. Kear, J. M. Oblak, and A. F. Giamei, *ibid*, p. 1155.
98. S. C. Huang, A. I. Taub, and K. M. Chang, *Acta Metall.* **32**, 1703 (1984).

99. H. G. Bohn, J. M. Williams, J. H. Barrett, and C. T. Liu, "Lattice Location of Boron and Hafnium Dupants in an Ordered Nickel Aluminide by Use of Ion Channeling/Nuclear Reaction Analyses," p. 127-33 in *High-Temperature Ordered Intermetallic Alloys, Materials Research Society Symposia Proceedings*, Vol. 81, eds. N. S. Stoloff, C. C. Koch, C. T. Liu, and O. Izumi, Materials Research Society, Pittsburgh, Pa., 1987.
100. P. H. Thornton, R. G. Davies, and T. L. Johnson, *Metall. Trans.* **1**, 207 (1970).
101. T. Ito and Y. Nakayama, *Scr. Metall.* **20**, 1141 (1986).
102. S. M. Copley and B. H. Kear, *Trans. The Metall. Soc., Am. Inst. Min., Metall. Pet. Eng.* **239**, 977 (1967).
103. C. Lall, S. Chin, and D. P. Pope, *Metall. Trans.* **10A**, 1323 (1979).
104. S. S. Ezz, D. P. Pope, and V. Paidar, *Acta Metall.* **30**, 921 (1982).
105. M. K. Miller and J. A. Horton, *Scr. Metall.* **20**, 1125 (1986).
106. J. Bentley, *Proc. 44th Electron Microscopy Society of America*, ed., E. W. Bailey, San Francisco Press, San Francisco, Calif., 1986, p. 704.

INTERNAL DISTRIBUTION

1-2.	Central Research Library	28.	T. G. Kollie
3.	Document Reference Section	29-33.	C. T. Liu
4-5.	Laboratory Records Department	34.	C. G. McKamey
6.	Laboratory Records, ORNL RC	35.	M. K. Miller
7.	ORNL Patent Section	36.	D. F. Pedraza
8.	D. J. Alexander	37.	W. D. Porter
9.	L. F. Allard	38.	A. C. Schaffhauser
10.	P. F. Becher	39.	J. H. Schneibel
11.	J. Bentley	40.	R. W. Swindeman
12.	P. J. Blau	41-43.	P. T. Thornton
13.	D. F. Craig	44.	P. F. Tortorelli
14.	S. A. David	45.	J. R. Weir
15.	J. H. DeVan	46.	J. M. Williams
16.	J. P. Forester	47-51.	M. H. Yoo
17.	E. P. George	52.	S. J. Zinkle
18-22.	J. A. Horton	53.	H. D. Brody (Consultant)
23.	C. Hsueh	54.	G. Y. Chin (Consultant)
24.	J. R. Keiser	55.	F. F. Lange (Consultant)
25.	E. A. Kenik	56.	W. D. Nix (Consultant)
26.	H. E. Kim	57.	D. P. Pope (Consultant)
27.	O. F. Kimball	58.	E. R. Thompson (Consultant)

EXTERNAL DISTRIBUTION

59. AFWAL MATERIALS LABORATORY, Wright-Patterson AFB, OH 45433-6533
D. M. Dimiduk
60. ALUMINUM COMPANY OF AMERICA LABORATORIES, Alcoa Technical Center,
Route 780, Seventh Street Road, Alcoa Center, PA 15269
G. MacZura
61. BROWN UNIVERSITY, Providence, RI 02912
R. J. Asaro
- 62-63. CAMBRIDGE UNIVERSITY, Cambridge CB21PZ, United Kingdom
M. F. Ashby
R. W. Cahn

- 64-65. CARNEGIE-MELLON UNIVERSITY, Department of Metallurgical Engineering
and Materials Science, Pittsburgh, PA 15213
T. B. Massalski
J. C. Williams
66. CASE WESTERN RESERVE UNIVERSITY, Cleveland, OH 44106
K. Vedula
- 67-68. COLUMBIA UNIVERSITY, New York, NY 10027
J. M. Sanchez
J. K. Tien
69. CZECHOSLOVAK ACADEMY OF SCIENCES, Prague 8, Czechoslovakia
V. Paidar
- 70-71. DARTMOUTH COLLEGE, Hanover, NH 03755
I. Baker
E. M. Schulson
72. COMMISSION OF THE EUROPEAN COMMUNITIES, Petten Establishment,
Postbus 2, 1755 ZG Petten, The Netherlands
Marcel Van de Voorde
73. EOTVOS UNIVERSITY, Budapest, Hungary
G. Tichy
- 74-75. ECOLE POLYTECHNIQUE FEDERALE DE LAUSANNE, CH-1015 Lausanne,
Switzerland
B. Ilschner
J. L. Martin
- 76-77. EG&G IDAHO, INC., Idaho National Engineering Laboratory,
P.O. Box 1625, Idaho Falls, ID 83415
J. E. Flinn
R. N. Wright
- 78-81. ELECTRIC POWER RESEARCH INSTITUTE, 3412 Hillview Avenue,
P.O. Box 10412, Palo Alto, CA 94303
W. T. Bakker
D. J. Frey
R. I. Jaffee
J. Stringer
82. GENERAL ELECTRIC COMPANY, Quartz and Chemicals Department,
24400 Highland Road, Richmond Heights, OH 44413
G. W. Weber

- 83-84. HARVARD UNIVERSITY, Cambridge, MA 02138
J. W. Hutchinson
J. R. Rice
85. IMPERIAL COLLEGE, London 3W72AZ, United Kingdom
D. G. Pettifor
86. INSTITUTE OF DEFENSE ANALYSES, 1801 Beauregard Street, Alexandria,
VA 22311
T. F. Kearns
- 87-88. KERNFORSCHUNGSANLAGE JÜLICH, F.R.G.
W. Schilling
H. Trinkaus
89. KYOTO UNIVERSITY, Sakyo-ku, Kyoto, Japan
M. Yamaguchi
90. LABORATORIE DE METALL. PHYS., 86022 Poitiers, Cedex, France
P. Veyssiére
91. LEHIGH UNIVERSITY, Materials Research Center, Bethlehem, PA 18015
Y. T. Chou
92. LEM, CNRS-ONERA, 92322 Châtillon Cedex, France
T. Khan
- 93-94. LOCKHEED CORPORATION, Palo Alto Laboratories, 3251 Hanover Street,
Palo Alto, CA 94303
E. C. Burke
T. G. Nieh
- 95-97. LOS ALAMOS NATIONAL LABORATORY, Los Alamos, NM 87545
S. P. Chen
P. J. Hay
R. S. Skaggs
- 98-100. MASSACHUSETTS INSTITUTE OF TECHNOLOGY, 77 Massachusetts Avenue,
Room 13-5026, Cambridge, MA 02139
S. M. Allen
A. S. Argon
W. S. Owen
- 101-102. MAX-PLANCK-INSTITUT FÜR EISENFORSCHUNG, 4000 Düsseldorf, F.R.G.
P. Neumann
G. Sauthoff

- 103-104. MICHIGAN TECHNOLOGICAL UNIVERSITY, Houghton, MI 49931
J. K. Lee
C. L. White
105. MONSANTO COMPANY, P.O. Box 1311, Texas City, TX 77590
P. S. Gupton
- 106-107. NATIONAL BUREAU OF STANDARDS, Gaithersburg, MD 20899
J. W. Cahn
R. Thomson
- 108-109. NAVAL RESEARCH LABORATORY, Washington, DC 20375-5000
M. S. Duesberry
K. Sadananda
110. NORTH CAROLINA STATE UNIVERSITY, Materials Engineering Department,
Raleigh, NC 27650
C. C. Koch
- 111-112. NORTHWESTERN UNIVERSITY, Evanston, IL 60201
A. J. Freeman
M. Meshii
- 113-115. OXFORD UNIVERSITY, Oxford OX13PH, United Kingdom
P. M. Hazzledine
P. B. Hirsch
A. P. Sutton
116. RENSSELAER POLYTECHNIC INSTITUTE, Materials Engineering Department,
Troy, NY 12181
N. S. Stoloff
- 117-118. RUTGERS UNIVERSITY, Department of Ceramics, P.O. Box 901,
Piscataway, NJ 08854
B. H. Kear
J. B. Wachtman, Jr.
- 119-122. SANDIA NATIONAL LABORATORIES, Livermore, CA 94550
M. I. Baskes
M. S. Daw
S. M. Foiles
M. J. Mills
123. TECHNISCHE UNIVERSITÄT, Hamburg-Harburg, F.R.G.
H. Mecking

124. THE UNIVERSITY OF TOKYO, Minato-ku, Tokyo, Japan
S. Takeuchi
- 125-126. TOHOKU UNIVERSITY, Institute of Materials Research, Sendai 980,
Japan
S. Hanada
O. Izumi
127. TOKYO INSTITUTE OF TECHNOLOGY, Midori-Ku, Yokohama 227, Japan
T. Suzuki
- 128-129. UNIVERSITY OF BIRMINGHAM, Birmingham B152TT, United Kingdom
M. Loretto
R. E. Smallman
- 130-132. UNIVERSITY OF CALIFORNIA, Berkeley, CA 94720
D. deFontaine
A. G. Khachaturyan
J. W. Morris, Jr.
133. UNIVERSITY OF CONNECTICUT, Storrs, CT 06268
P. C. Clapp
- 134-135. UNIVERSITY OF GRONINGEN, 9747 AG Groningen, The Netherlands
J. Th. M. DeHosson
A. W. Slecswyk
136. UNIVERSITY OF MASSACHUSETTS, Department of Polymer Science,
Room 701, GRC, Amherst, MA 01003
R. S. Porter
- 137-138. UNIVERSITY OF MICHIGAN, Ann Arbor, MI 48109
R. Gibala
D. J. Scolovitz
- 139-140. UNIVERSITY OF PENNSYLVANIA, 3231 Walnut Street,
Philadelphia, PA 19104
D. P. Pope
V. Vitek
- 141-142. UNIVERSITY OF VIENNA, Vienna 7090, Austria
H. Kirchner
A. Korner
143. URALS SCIENTIFIC CENTER, Academy of Sciences, U.S.S.R.
B. A. Grinberg

144. VANDERBILT UNIVERSITY, Station B, P.O. Box 1621,
Nashville, TN 37235
J. J. Wert
145. VIRGINIA POLYTECHNIC INSTITUTE AND STATE UNIVERSITY, Blacksburg,
VA 24061
D. A. Farkas
- 146-148. DOE, ENERGY SYSTEMS RESEARCH AND DEVELOPMENT, Office of
Conservation and Renewable Energy, Forrestal Building,
Independence Avenue, Washington, DC 20585
J. J. Brogan
J. J. Eberhardt
S. M. Wolf
- 149-152. DOE, MORGANTOWN ENERGY TECHNOLOGY CENTER, P.O. Box 880,
Morgantown, WV 26505
D. Dubis
M. Ghate
J. M. Hobday
J. S. Wilson
153. DOE, OAK RIDGE OPERATIONS, P.O. Box 2001, Oak Ridge, TN 37831
Assistant Manager for Energy Research and Development
- 154-156. DOE, OFFICE OF BASIC ENERGY SCIENCES, Material Sciences Division,
Washington, DC 20545
J. B. Darby, Jr.
F. V. Nolfi, Jr.
I. L. Thomas
- 157-162. DOE, OFFICE OF FOSSIL ENERGY, Washington, DC 20545
J. P. Carr
C. Garrett
R. E. Harrington
L. Naphtali
P. Scott
T. B. Simpson
163. DOE, OFFICE OF VEHICLE AND ENGINE R&D, Route Symbol CE-131,
Forrestal Building, Washington, DC 20585
R. B. Schulz
- 164-215. DOE, OFFICE OF SCIENTIFIC AND TECHNICAL INFORMATION,
P.O. Box 62, Oak Ridge, TN 37831
For distribution as shown in DOE/TIC-4500, Distribution
Category UC-404 (Materials).